Reviews of Modern Plasma Physics (2022) 6:11
https://doi.org/10.1007/s41614-022-00072-6

REVIEW PAPER

Trapping in quantum plasmas: a review

W. Masood[1,2] · H. A. Shah[3] · M. N. S. Qureshi[4]

Received: 10 November 2021 / Accepted: 16 April 2022 / Published online: 17 May 2022

Abstract
In this paper, we have presented a comprehensive review of electron trapping in quantum plasmas. We have begun by giving a brief introduction of electron trapping in classical plasmas and then derived the expression of number density of trapped electrons for non-relativistic and relativistically degenerate cases and quantizing magnetic field. We have obtained the expression for Sagdeev potential for all these cases and explored the variation of solitary structures with the important plasma parameters. We have also derived the equations for drift ion acoustic and pure drift waves for spatially nonuniform quantum magnetoplasmas both in collisionless and collisional plasmas. The fundamental differences in trapping in classical and quantum plasmas have been enunciated in detail. The applications of the work in ultra-strong laser plasma interactions and white dwarf stars have also been pointed out.

Keywords Quantum plasmas · Trapping · Solitary waves · Shock waves · Fluid theory · Sagdeev potential

1 Introduction

More than 60 years ago, Klimontovich (1952), Bohm (1952) and Bohm and Pines (1953) in their seminal papers laid the foundations of the study of quantum plasmas and collective oscillations. These works were based on the pioneering work of Chandrasekhar (1931) where the degenerate nature of electrons was recognized in astrophysical objects. These early works were followed by the famous paper by

✉ W. Masood
waqasmas@gmail.com

[1] Department of Physics, COMSATS University Islamabad (CUI), Islamabad Campus, Park Road, Chak Shahzad, Islamabad 44000, Pakistan

[2] National Centre for Physics (NCP), Shahdara Valley Road, P.O. Box 2141, Islamabad 44000, Pakistan

[3] Department of Physics, FC College (A Chartered University), Ferozepur Road, Lahore 54600, Pakistan

[4] Department of Physics, GC University, Katchery Road, Lahore 54000, Pakistan

Pines (1961) which paved the way for investigating collective interactions in quantum solid-state plasma. Some early works in this direction accounted for quantum corrections and made analytical and numerical investigations (Shokri and Rukhadze, 1999a, b; Shokri and Khorashady 2003; Luque et al. 2004). Such plasmas are degenerate, have high number densities and low temperatures and are described by the Fermi–Dirac distribution function. In such plasmas, due to their very high densities, the average interparticle distance, which can be estimated through the number density, and is taken as $\sim n_e^{-1/3}$, decreases and becomes comparable to the de Broglie wavelength $\lambda_B = \hbar/\left(2\pi m_e T\right)^{1/2}$ where m_e is the mass and T the temperature in energy units and $n_e\lambda_B \geq 1$ [see for, e.g. Haas (2011)]. In such a situation, the Fermi temperature becomes much larger than the ambient temperature and consequently quantum effects begin to play a defining role in the collective interactions of the plasma. Degenerate or quantum plasma gained importance due to its applications in plasma effects in semiconductor and metals (Markowich et al. 2012), quantum wells, quantum dots and quantum nanotubes (Ang et al. 2003). A large volume of literature has been published covering both theoretical and experimental aspects of quantum degenerate plasmas [see for instance, the reviews by Shukla and Eliasson (2010a, b)] and the most fundamental of these has been the paper by Manfredi (2005) which gave an excellent introduction on 'how to study quantum plasmas'. In the past decade or so, degenerate plasmas have been extensively studied due to their wide ranging applications in very diverse areas ranging from solid-state plasmas [nanophysics, nanoplasmonics semiconductor lasers (Luque et al. 2004; Yalabik et al. 1989; Luscombe et al. 1992; Manfredi and Hervieux 2007; Yahia et al. 2013; Haug and Koch 2009)] on the small scale and dense astrophysical plasmas like active galactic nuclei, neutron stars, etc., on the very large scale (Horn 1991; Chabrier et al. 2002).

The expansion of a quantum gas into vacuum, quantum plasma echoes, Landau damping in quantum systems and streaming instabilities have all been subjects of interest in quantum plasmas (Suh et al. 1991; Mola et al. 1993; Manfredi and Feix 1996; Haas et al. 2000; Ali and Shukla 2007; Shukla et al. 2008). Quantum hydrodynamical plasmas have been the subject of investigation in both the linear and nonlinear regimes taking into account solitary waves and effects due to spin of the electrons (Haas 2011; Shukla and Stenflo 2006; Ali et al. 2007; Haque and Saleem 2008; Mahmood and Mushtaq 2008; Mushtaq and Qamar 2009; Sah and Manta 2009; Shukla and Eliasson 2011; Haas and Mahmood 2016). Nonlinearities in relativistic classical plasmas have been studied since the 1970s, e.g. Demchenko and El-Naggar (1972) who considered nonlinear forced longitudinal oscillations in a relativistic plasma. In Ref. Tsintsadze and Tsikarishvili (1976), transport phenomena in ultra-relativistic plasmas were investigated and in Ref. Chian (1982), the role of ion dynamics on relativistic oscillations was investigated. Solitons in relativistic plasmas were first investigated in Ref. Tsintsadze and Tskhakaya (1977) where the authors derived the Korteweg de Vries (KdV) equation. For relativistic streaming ions, Nejoh derived the KdV equation Nejoh (1992). The development of the Sagdeev potential approach made it possible to consider arbitrary amplitude waves (Strasser 1996; Sahu and Roychoudhury 2004, 2006). The fully relativistic two-fluid model was employed in a streaming plasma and propagation of arbitrary amplitude solitary structures was studied using the Sagdeev potential approach (Lee and Choi

2007). These studies have been gainfully employed to investigate formation of solitary structures in laser plasma interactions (Kuehl and Zhang 1991) and space plasmas (Mahmood and Masood 2008). More recently, quantum hydrodynamic (QHD) model has been successfully used to comprehend different topics related to linear and nonlinear propagation of waves in dense degenerate plasmas (Ren et al. 2009; Masood et al. 2009; Masood 2009a, b). These plasmas have engendered interest because of their interesting applications in stellar environments, laser plasma interactions and in microelectronic devices.

The relativistic effects come into play when the number densities go in excess of 10^{32} m^{-3} as the Fermi speed becomes comparable with the speed of light. Such high densities are found in superdense astrophysical objects like white dwarf stars (Balberg and Shapiro 2000a, b). Helium, carbon and oxygen are most frequently found in the interior of white dwarf stars (Chatterjee et al. 2009). The examples of relativistically degenerate plasmas include active galactic nuclei, pulsar and neutron star magnetospheres, quasars and accretion discs (Michel 1982; Orosz et al. 1997; Goldreich and Julian 1969; Daniel and Tajima 1998). Recently in Ref. Tsintsadze et al. (2009), nonlinear static screening in ultra-relativistic electron positron plasmas was studied and comparison was made with the Debye and Coulomb screening results. The likelihood of the formation of bound structures and the part that electrostatic fluctuations play was also discussed.

Nonlinear aspects have covered shock waves (Masood et al. 2009, 2010, 2014), nonlinear dynamics and chaotic evolution (Shukla et al. 2011; Zobaer et al. 2013; Saha et al. 2020). On the other hand, the kinetic approach has also been studied using the Wigner Moyal (Tyshetskiy et al. 2013) formulation leading to a modified Vlasov equation approach. In classical plasmas, a special type of a nonlinearity was studied by Bernstein et al. (1957), Luque and Schamel (2005) where it was shown that trapped particles can significantly influence the nonlinear properties of plasma waves; however, in this instance the wave itself captured or trapped the particles. Ten years later, Gurevich (1968) treated trapping as a microscopic phenomenon when he considered the distribution of electrons in a slowly varying potential. This has been discussed in some considerable detail in Ref. Pitaevskii and Lifshitz (2012) by considering L to be the extent of the field and τ the characteristic time of the variation of the field and v_e the velocity of the electrons as it passes through the potential field. Thus if $\tau \gg L/v_e$, then the potential could be considered slowly varying for which there is an adiabatic invariant expressed through the integral $I(t,\epsilon) \sim \int_a^b [2m(\epsilon - U(t,x)]\mathrm{d}x$, which leads to the possibility of part of the electrons being adiabatically captured as a microscopic process. Adiabatic trapping separates the electron distribution into two parts—the free electron part and the trapped electron part. Here, two cases may occur—when the potential well is deep and when the potential well is shallow. In the case of the deep potential well, $n_e = 2n_0\left(\frac{U}{\pi T}\right)^{1/2}$ and in the case of the shallow potential $n_e = n_0\left[1 + \frac{U}{T} - \frac{4}{3\sqrt{\pi}}\left(\frac{U}{T}\right)^{\frac{3}{2}}\right]$, where U is the potential energy and n_e and n_0 are the total and unperturbed number densities respectively. It has been shown that the effect of the adiabatically trapped electrons in a shallow potential lead to a 3/2

power nonlinearity. In the same paper, Gurevich (1968) studied ion acoustic waves with the effect of adiabatically captured electrons in a shallow potential well and obtained a modified KdV equation with a 3/2 order nonlinearity instead of the usual quadratic nonlinearity and this had a solution proportional to $\mathrm{sech}^4 \kappa x$ instead of the usual $\mathrm{sech}^2 \kappa x$ solution in a co-moving frame of reference. The case of the deep potential well has been of less interest as the result predicted shows that almost the entire plasma is trapped in the potential well. Experiments and computer simulations (Sagdeev and Leontovich 1966) carried out later confirmed the theoretical results predicted by Gurevich (1968). Thus, Gurevich's paper is considered a watershed in the development of fractional power nonlinearities.

Over the years, several authors have investigated the effect of adiabatic trapping in classical plasmas using both Maxwellian (Abbasi et al. 1999; Ayub et al. 2011; Shah et al. 2014) and non-Maxwellian distributions (Mushtaq and Shah 2006) leading to modified soliton solutions. In most cases, these nonlinear structures have been investigated using the Sagdeev potential approach (Leontovich 2012). The trapping effect has also been investigated for vortices and in this case a modified Hasegawa–Mima equation (Siddiqui et al. 2008) was obtained. Most of the work mentioned above considered the adiabatic capture effect for ion acoustic waves; however, coupled kinetic Alfven-ion acoustic waves were investigated in Shah et al. (2013). This interest has been motivated by the importance which nonlinear problems in physics and other disciplines have evoked ever since the discovery of the solitary wave or solitons.

In quantum or degenerate plasmas, nonlinear problems remain on the forefront of investigations and a large volume of literature has emerged covering different types of solitary and shock structures [see references above]. However, the role which trapping may play in the formation and propagation of solitary structures has received considerably less attention. We point out here that one of the earliest papers which took trapping into account was work done by Luque and Schamel (2005) who investigated the effect of quantum corrections in electron hole plasmas by using a perturbative technique to the Wigner Poisson set of equations. Later, Demeio (2007) considered trapping for the Bernstien Greene Kruskal (BGK) equilibria and investigated the effect of trapping in quantum phase space. However, work on adiabatic trapping by Gurevich (1968) in degenerate plasmas was first initiated by Shah et al. (2010) about a decade ago and since then a number of different aspects of adiabatic electron capture have been investigated on the propagation of nonlinear waves and these will be the subject of review in the ensuing sections. It was seen that a novel nonlinearity which is of the form $(1+\phi)^{3/2}$ appears. Subsequently, several different aspects of adiabatic trapping have been investigated which include both relativistic and non-relativistic regimes, the effects of Landau quantization, the role of positrons, etc. In the current review, we hope to cover most of these studies—most of which have been carried out by our group.

The layout of our work is as follows: In Sect. 2, we give the mathematical preliminaries of the electron distribution function for free and adiabatically trapped parts. In Sect. 3, we present the results of linear dispersion relation and nonlinear evolution equation for quantum ion acoustic waves with adiabatically trapped electrons

and the analytical and graphical results of the corresponding Sagdeev potential. In Sect. 4, we present the relativistic case for quantum ion acoustic waves.

2 Mathematical preliminaries of electron trapping in quantum plasmas

In this section, we briefly explain the procedure to obtain the expression for the adiabatically trapped number density of partially degenerate electrons following Ref. Kuehl and Zhang (1991). The electron energy in a potential field, ϕ, is given by $\varepsilon = \frac{p^2}{2m} + u$, where p is the momentum while m is the mass of the electrons and $u = -e\phi$ is the trapping potential. Energy $\varepsilon > 0$ is for the free, whereas $\varepsilon < 0$ is the energy of the trapped electrons. Trapping happens when the condition $\varepsilon = 0$ is fulfilled.

Since the electrons behave quantum mechanically, they are assumed to follow the Fermi Dirac distribution function. To find the total electron number density in a potential field, we make use of the spherical polar coordinates and upon integrating and shifting to energy variables arrive at the following expression:

$$n_e(r,t) = \frac{8\pi\sqrt{2}m^{\frac{3}{2}}}{(2\pi\hbar)^3}\int_0^\infty \frac{\varepsilon^{\frac{1}{2}}\mathrm{d}E}{e^{\frac{\varepsilon-\mu-e\varphi}{T}}+1}. \tag{1}$$

Here μ is the chemical potential, T is the system temperature and e is the electron charge. Setting $U = \mu + e\varphi$, then for trapped particles we have the following condition $\varepsilon - U = 0$. Equation (1) can be solved using the reference Landau and Lifshitz (1980), but some main steps are given below. Making a change of variables $\frac{\varepsilon-U}{T} = z$ and after some algebraic manipulation, we obtain

$$n_e(r,t) = \frac{8\pi\sqrt{2}m^{3/2}}{(2\pi\hbar)^3}T\left[\int_0^{U/T}(U-Tz)^{1/2} + \int_0^{\varepsilon}\frac{(U+Tz)^{1/2}-(U-Tz)^{1/2}}{e^z+1}\mathrm{d}z\right]. \tag{2}$$

The first and second integrals represent the effects of trapped and untrapped electrons, respectively. These integrals are dealt with separately. The first integral can be solved in the straightforward way, and it will give the following result:

$$\int_0^{U/T}(U-Tz)^{1/2} = \frac{2}{3T}U^{3/2}. \tag{3}$$

The second integral is solved by using the standard procedure of solving the Fermi Dirac integrals (Landau and Lifshitz 1980; Pointon 1980). In the small temperature limit and incorporating Eq. (3), we obtain

$$n_e(r,t) = \frac{8\pi\sqrt{2}m^{\frac{3}{2}}}{(2\pi\hbar)^3}\left[\frac{2}{3}U^{\frac{3}{2}} + \frac{\pi^2T^2}{12}U^{-\frac{1}{2}}\right]. \tag{4}$$

We note that the temperature is taken to be small compared to the Fermi temperature (or Fermi energy). We further note that for a fully degenerate plasma, i.e., for $T = 0$, $\mu = \varepsilon_F = \frac{\hbar^2}{2m_e}\left(3\pi^2 n\right)^{2/3}$. Note that μ is not exactly equal to ε_F when $T \neq 0$. Hence $U = \varepsilon_F + e\varphi$ and so the above equation can be written as

$$n_e(r,t) = \frac{8\pi\sqrt{2}m^{\frac{3}{2}}}{(2\pi\hbar)^3}\left[\frac{2}{3}\left(\varepsilon_F + e\varphi\right)^{\frac{3}{2}} + \frac{\pi^2T^2}{12}\left(\varepsilon_F + e\varphi\right)^{-\frac{1}{2}}\right], \tag{5}$$

which can finally be expressed in the following form:

$$n_e(r,t) = n_0\left[(1+\Phi)^{\frac{3}{2}} + T^2(1+\Phi)^{-\frac{1}{2}}\right]. \tag{6}$$

Here n_0 is the total background number density. The temperature T and the potential Φ are normalized as

$$\Phi = \frac{e\varphi}{\varepsilon_F} \text{ and } T = \frac{\pi T}{2\sqrt{2}\varepsilon_F} \text{ where } \frac{T}{\varepsilon_F} \ll 1.$$

For fully degenerate plasmas and in the absence of perturbation, the number density reads as $n_{0e} = n_0 = n_{0i}$. The temperature T denotes partial degeneracy and is always taken to be small for quantum plasmas.

The expression representing the number density of electrons experiencing adiabatic trapping forms the backbone of further considerations for trapping problems in quantum degenerate plasmas. In absence of the potential Φ, Eq. (6) reduces to the standard expression of density for partially degenerate electrons (Pointon 1980). We now also note that the nonlinearity occurring in a quantum plasma is of a novel form, i.e., $(1+\Phi)^{3/2}$ whereas in a classical plasma the nonlinearity due to adiabatic trapping is of the form $\Phi^{3/2}$ and this difference significantly modifies the properties of the nonlinear structures. Although in the subsequent sections, we will consider relativistic problems and the effects of a quantizing magnetic field, the brief description of the integration given above for adiabatically trapped electrons in a degenerate plasma remains in general the same.

3 Ion acoustic waves in relativistic and non-relativistic degenerate plasma with adiabatically trapped electrons

In this section, we will give an overview of the early work [Refs. Shah et al. (2010), Shah et al. (2011)] on adiabatic capture in dense degenerate plasmas. In our papers Shah et al. (2010), Shah et al. (2011)), we have considered the effects of adiabatic trapping of electrons on ion acoustic waves in both non-relativistic and relativistic plasmas. In the section below, we give a general outline of the work on relativistic

degenerate plasmas and present the results of our first paper (Shah et al. 2010) as limiting case of Shah et al. (2011). In Sect. 3.1, we present the governing equations to study the linear ion acoustic waves (IAWs) for relativistically degenerate trapped electrons and cold classical ions. We shall also present the limiting cases (i.e., non-relativistic and ultra-relativistic) and briefly discuss them. In Sect. 3.2, we present the nonlinear analysis employing the Sagdeev potential approach. In order to differentiate between the relativistic, non-relativistic and ultra-relativistic cases, we have used the subscripts R, N and U in the entire text. In the subsequent subsections, we shall give numerical analysis of our results.

3.1 Mathematical preliminaries and linear dispersion relations

We follow the method outlined in Sect. 2 to arrive at the number density of adiabatically trapped relativistic electrons. The relativistic electron energy in the presence of a potential field, ϕ, is given by $\varepsilon = c\sqrt{p^2 + m_0^2 c^2} + u$, where momentum is denoted by p, m_0 denotes the rest mass of the electrons and $u = -e\phi$ is the trapping potential. The rest of the details are the same as given in Sect. 2. Thus, the expression for the total number density of electrons for the relativistically degenerate case reads as

$$n_{\mathrm{eR}} = \frac{\mu^3}{3\pi(\hbar c)^3}\left[\left\{\left(1+\Phi_{\mathrm{R}}\right)^2 - \varepsilon_0^2\right\}^{3/2} + \frac{\pi^2 T_{\mathrm{R}}^2}{6}\frac{\left\{2\left(1+\Phi_{\mathrm{R}}\right)^2 - \varepsilon_0^2\right\}}{\left\{\left(1+\Phi_{\mathrm{R}}\right)^2 - \varepsilon_0^2\right\}^{1/2}}\right] \tag{7}$$

In this case, $\mu = \varepsilon_{F0} + m_0 c^2$ is the chemical potential in the relativistic case which is a permissible approximation in the low-temperature case, and $\varepsilon_{F0} = \left(3\pi^2 n_0\right)^{2/3}\frac{\hbar^2}{2m}$, $\Phi_{\mathrm{R}} = e\varphi/\mu$ denotes the normalized relativistic potential, $T = T/\mu$ is the normalized temperature, and the normalized total energy is $\varepsilon_0 = m_0 c^2/\mu$. The absence of trapping potential, Φ_{R} gives $n_{eR} = n_{0R}$, where

$$n_{0R} = \frac{\varepsilon_{F0}^3}{3\pi(\hbar c)^3}\left[\left(1-\varepsilon_0^2\right)^{3/2} + \frac{\pi^2 T_{\mathrm{R}}^2\left(2-\varepsilon_0^2\right)}{6\left(1-\varepsilon_0^2\right)^{1/2}}\right] \tag{8}$$

for relativistically degenerate electrons.

On account of their three orders of magnitude higher mass than electrons, the ions are assumed to behave in a classical manner and are further considered to be cold. The equations of motion and continuity for the ions read as

$$m_i n_i\left(\frac{\partial}{\partial t} + \vec{v}_i.\overrightarrow{\nabla}\right)\vec{v}_i = -e\vec{\nabla}\phi \tag{9}$$

$$\frac{\partial}{\partial t}n_i + \vec{\nabla}\cdot n_i\vec{v}_i = 0 \tag{10}$$

and the Poisson's equation reads as

$$\nabla^2\varphi = 4\pi e\left(n_e - n_i\right). \tag{11}$$

In order to study the nonlinear behaviorr of IAWs, we transform ourselves to a frame that travels at the speed of the nonlinear structure u, i.e., $\xi = x - ut$, and integrate the equations above using the boundary conditions (BCs), namely when $\xi \to \infty$, v_i and $\phi \to 0$, and $n_i \to n_0$, where the equilibrium number density of electrons and ions for a degenerate plasma is denoted by n_0, to obtain

$$n_i = n_{0R}\left(1 - \Phi_R/M_R^2\right)^{-1/2} \tag{12}$$

Here $M_R = \sqrt{m_i u^2/2\mu}$ we now substitute the above in Poisson's equation (Eq. (11)) and obtain

$$\frac{\mathrm{d}^2\Phi_R}{\mathrm{d}\xi^2} = \frac{4\pi e^2 n_{0R}}{\mu}\left[\frac{\left\{\left(1+\Phi_\mathrm{R}\right)^2 - \varepsilon_0^2\right\}^{3/2} + \frac{\pi^2T^2}{6}\frac{\left\{2\left(1+\Phi_\mathrm{R}\right)^2 - \varepsilon_0^2\right\}}{\left\{\left(1+\Phi_\mathrm{R}\right)^2 - \varepsilon_0^2\right\}^{1/2}}}{n_{0R}} - \left(1 - \frac{\Phi_\mathrm{R}}{M_\mathrm{R}^2}\right)^{-1/2}\right]. \tag{13}$$

Linearization of Eqs. (7), (11) and (13) and using the definition of M_R given above and defining $u = \omega/k$ yields the following dispersion relation of IAWs in a relativistically degenerate plasma:

$$\omega = kc_{sR}\sqrt{\frac{1}{1 + k^2\lambda_{TF,R}^2}}, \tag{14}$$

where $\lambda_{TF,R} = \sqrt{\frac{\mu}{4\pi e^2 n_{0R}A_R}}$ is the screening length and $c_{sR} = \sqrt{\frac{\mu}{m_i A_R}}$ is the acoustic speed in a relativistically degenerate plasma and

$$A_R = \frac{3\left\{(1-\varepsilon_0^2)^{1/2} + \frac{\pi^2T^2(2-3\varepsilon_0^2)}{18(1-\varepsilon_0^2)^{1/2}}\right\}}{(1-\varepsilon_0^2)^{3/2} + \frac{\pi^2T^2(2-\varepsilon_0^2)}{6(1-\varepsilon_0^2)^{1/2}}}, \tag{15}$$

which contains terms that reflect the relativistic and temperature correction effects. Making use of Eq. (14), the general definition of the Mach number is expressed as

$$\mathscr{M}_R = M_R\sqrt{A_R}. \tag{16}$$

3.2 Limiting cases

Next, we discuss the non-relativistic case ($m_0c^2 >> \varepsilon_{F0}$) and the ultra-relativistic ($m_0c^2 << \varepsilon_{F0}$) limits. Equation (5), in the non-relativistic limit reads as

$$n_{eN} = \frac{\left(2m_0\varepsilon_{F0}\right)^{3/2}}{3\pi^2\hbar^3}\left[\left(1+\Phi_N\right)^{3/2} + \frac{\pi^2 T_N^2}{24}\left(1+\Phi_N\right)^{-1/2}\right], \tag{17}$$

which is the same expression which was reported in our paper (Shah et al. 2010) with the exception of the difference in the normalization of T. Thus, in the non-relativistic limit, $\mu = \varepsilon_{F0}$, $T_N = \pi T/\varepsilon_{F0}$ and $\Phi_N = e\varphi/\varepsilon_{F0}$. The expression for the limiting non-relativistic number density when no perturbation is present reads as

$$n_{0N} = \frac{\left(2m_0\varepsilon_{F0}\right)^{3/2}}{3\pi^2\hbar^3}\left[1 + \frac{\pi^2 T_N^2}{24}\right] \tag{18}$$

Using Eqs. (9) and (15) in Eq. (10) and using Eq. (16)

$$\frac{\mathrm{d}^2\Phi_N}{\mathrm{d}\xi^2} = \frac{4\pi e^2 n_{0N}}{\varepsilon_{F0}}\left[\frac{\left\{\left(1+\Phi_N\right)\right\}^{3/2} + \frac{\pi^2 T_N^2}{24}\left\{1+\Phi_N\right\}^{-1/2}}{n_{0N}} - \left(1 - \frac{\Phi_N}{M_N^2}\right)^{-1/2}\right]. \tag{19}$$

Assuming sinusoidal perturbation and following the method adopted for the relativistic case, and defining Mach number in the non-relativistic case as $M_N = \sqrt{m_i u^2/2\varepsilon_{F0}}$, the linear dispersion relation of IAWs with the inclusion of small temperature corrections gives

$$\omega = kc_{sN}\sqrt{\frac{1}{1+k^2\lambda_{TF,N}^2}}, \tag{20}$$

where $\lambda_{TF,N} = \sqrt{\frac{\varepsilon_{F0}}{4\pi e^2 n_{0N} A_N}}$ is the screening length and $c_{sN} = \sqrt{\frac{2\varepsilon_{F0}}{m_i A_N}}$ is the sound velocity for the non-relativistic case.

$$A_N = \frac{3(1+\pi^2T^2/24)}{(1-\pi^2T^2/72)}. \tag{21}$$

Note that the factor A_N contains the temperature corrections. The non-relativistic Mach number reads as

$$\mathscr{M}_N = M_N\sqrt{A_N}. \tag{22}$$

In the ultra-relativistic case $m_0c^2 << \varepsilon_{F0}$ the number density given by Eq. (5) becomes

$$n_{eU} = \frac{\varepsilon_{F0}^3}{3\pi^2\hbar^3c^3}\left(1+\Phi_U\right)\left[\left(1+\Phi_U\right)^2 + \pi^2 T_U^2\right]. \tag{23}$$

The letter U denotes the ultra-relativistic case. It is appurtenant to mention here that we use ultra-relativistic number density to compute Fermi energy in this case. Moreover, ε_{F0} gets replaced by momentum p_F here and reads as $\varepsilon_{F0} = cp_F$. An important

observation is that unlike the fractional nature of nonlinearity in the relativistic and non-relativistic cases, the nature of nonlinearity is represented by whole number indices for the ultra-relativistic case. When the perturbation is not present, we have the following expression for number density of electrons:

$$n_{0U} = \frac{\left(2m_0\varepsilon_{F0}\right)^{3/2}}{3\pi^2\hbar^3}\left[1+\pi^2T_U^2\right]. \tag{24}$$

Substituting Eqs. (10) and (22) in (9), with appropriate normalization yields the following expression for the ultra-relativistic Poisson's equation:

$$\frac{\mathrm{d}^2\Phi_U}{\mathrm{d}\xi^2} = \frac{4\pi e^2 n_{0U}}{\varepsilon_{F0}}\left[\frac{\left(1+\Phi_U\right)\left\{\left(1+\Phi_U\right)^2\right\}+T_U^2}{n_{0U}} - \left(1-\frac{\Phi_U}{M_U^2}\right)^{-1/2}\right]. \tag{25}$$

Linearization of Eqs. (14) and (15) and the subsequent use of a plane wave solution yields the dispersion relation for the relativistic case

$$\omega = kc_{sU}\sqrt{\frac{1}{1+k^2\lambda_{TF,U}^2}}. \tag{26}$$

Here $c_{sU} = \sqrt{\varepsilon_{F0}/m_iA_U}$ is the ultra-relativistic sound velocity and the ultra-relativistic Thomas Fermi length is given by $\lambda_{TF,U} = \sqrt{\frac{\varepsilon_{F0}}{4\pi e^2 n_{0U}A_U}}$ and the temperature-dependent ultra-relativistic factor is given by

$$A_U = 3\left(1+\pi^2T_U^2/3\right)/\left(1+\pi^2T_U^2\right). \tag{27}$$

And the relativistic Mach number is

$$\mathscr{M}_U = M_U\sqrt{A_U}. \tag{28}$$

3.3 Sagdeev potential

In this section, we derive an expression for the Sagdeev potential in the relativistic case and obtain conditions for the existence of solitary waves by considering small temperature corrections when $T \neq 0$.

Using the analogy of a particle in a potential well and after integration and following Refs. Witt and Lotko (1983), Mamun (1997), we obtain from Eq. (13)

$$\frac{1}{2}\left(\frac{\mathrm{d}\Phi_\mathrm{R}}{\mathrm{d}\xi}\right)^2 + V_\mathrm{R}(\Phi_\mathrm{R}) = 0, \tag{29}$$

where the relativistic Sagdeev potential is given by

$$V_{\mathrm{R}} = -\frac{(-1+\epsilon_0^2)\left(\begin{array}{l}(-1+\epsilon_0^2)(-6-4\pi^2T_{\mathrm{R}}^2+15\epsilon_0^2)+8\mathrm{M}_{\mathrm{R}}^2\left(-\pi^2T_{\mathrm{R}}^2(-2+\epsilon_0^2)+6(-1+\epsilon_0^2)^2\right)\\ +9\epsilon_0^4\sqrt{1-\epsilon_0^2}\mathrm{Log}\left[1+\sqrt{1-\epsilon_0^2}\right]\end{array}\right)}{4\left(18\epsilon_0^4+2\left(9+\pi^2T_{\mathrm{R}}^2\sqrt{1-\epsilon_0^2}\right)-3\epsilon_0^2\left(12+\pi^2T_{\mathrm{R}}^2\sqrt{1-\epsilon_0^2}\right)\right)}$$
$$-\frac{\left(-T_{\mathrm{R}}^2(-2+\epsilon_0^2)+6(-1+\epsilon_0^2)^2\right)\left(\begin{array}{l}2M_{\mathrm{R}}^2\sqrt{1-\frac{\Phi_{\mathrm{R}}}{M_{\mathrm{R}}^2}}+\frac{\sqrt{1-\epsilon_0^2}(1+\Phi_{\mathrm{R}})\sqrt{-\epsilon_0^2+(1+\Phi_{\mathrm{R}})^2}\left(4\pi^2T_R^2-15\epsilon_0^2+6(1+\Phi_{\mathrm{R}})^2\right)}{4\left(-T_R^2(-2+\epsilon_0^2)+6(-1+\epsilon_0^2)^2\right)}\\ +\frac{9\epsilon_0^4\sqrt{1-\epsilon_0^2}\mathrm{Log}\left[1+\Phi_{\mathrm{R}}+\sqrt{-\epsilon_0^2+(1+\Phi_{\mathrm{R}})^2}\right]}{4\left(-\pi^2T^2(-2+\epsilon_0^2)+6(-1+\epsilon_0^2)^2\right)}\end{array}\right)}{18\sqrt{1-\epsilon_0^2}\left(\sqrt{1-\epsilon_0^2}+\frac{\pi^2T_{\mathrm{R}}^2\left(-2+3\epsilon_0^2\right)}{18\left(-1+\epsilon_0^2\right)}\right)} \tag{30}$$

We have found the integration constants using the BCs $\xi = \xi/\lambda_{\mathrm{TF},R} \to \infty$, $\Phi_R \to 0$. Moreover, as shown in Ref. Mamun (1997), Eq. (20) clearly shows that $V_{\mathrm{R}}(\Phi) = \frac{\mathrm{d}V_{\mathrm{R}}(\Phi)}{\mathrm{d}\Phi} = 0$ when$\Phi = 0$, and following the argument given in Ref. (Witt and Lotko 1983), we see that solitary waves solutions are obtained from Eq. (29) when the following two conditions are met: (i) if $(\mathrm{d}^2V_{\mathrm{R}}/\mathrm{d}\Phi_{\mathrm{R}}^2)_{\Phi_{\mathrm{R}}=0} < 0$, i.e., the fixed point is unstable at the origin and (ii) $V_R(\Phi_R) < 0$ $\mathrm{V}(\Phi) < 0$ $\mathrm{V}(\Phi) < 0$ when $0 < \Phi_{\mathrm{R}} < \Phi_{\mathrm{R\,max}}$ $0 < \Phi < \Phi_{\mathrm{max}}$. For nonlinear dip structures and for hump structures $V_R(\Phi_R) < 0$ when $0 > \Phi_{\mathrm{R}} > \Phi_{\mathrm{R\,min}}$. The cases for the existence of the solitary waves are discussed below. Using the Taylor expansion to expand the Sagdeev potential (see Eq. (30), we find the lower limit on the Mach number (Mamun 1997) by putting the coefficient of the quadratic term in $\Phi_R = 0$ to obtain

$$\mathscr{M}_{\mathrm{R,low}} = \frac{\left(\left(1-\varepsilon_0^2\right)^{3/2}+\frac{\pi^2T_{\mathrm{R}}^2}{18}\left(2-3\varepsilon_0^2\right)\right)}{A_{\mathrm{R}}}\sqrt{\frac{3\left(\left(1-\varepsilon_0^2\right)^2+\frac{\pi^2T_{\mathrm{R}}^2}{6}\left(2-\varepsilon_0^2\right)\right)}{2\left(\left(1-\varepsilon_0^2\right)^2+\frac{\pi^2T_{\mathrm{R}}^2}{18}\left(2-3\varepsilon_0^2\right)\right)}}. \tag{31}$$

We find the upper bound of $\mathscr{M}_R$ by using Eq. (12). The usual method is to find the range of $\mathscr{M}_R$ numerically for different values of ε_0 and T.

Like the previous section, the limiting cases of the relativistic case for the Sagdeev potential are considered. In the non-relativistic limit $m_0c^2 >> \varepsilon_{F0}$, Sagdeev potential reads as

$$V_N(\Phi_N) = -\frac{1}{\left(1-\pi^2T_N^2/72\right)}\left\{\begin{array}{l}\frac{\pi^2T_N^2}{18}\left(1+\Phi_N\right)^{1/2}+\frac{4}{15}(1+\Phi_N)^{5/2}+\frac{4M_N^2}{3}\left(1-\frac{\Phi_N}{M_N^2}\right)^{1/2}\left(1+\frac{\pi^2T_N^2}{24}\right)\\ -\frac{1}{90}\left(24+5\pi^2T_N^2\right)\left(1+5M_N^2\right)\end{array}\right\}. \tag{32}$$

The above expression retrieves the results of our paper (Shah et al. 2010), with a modification in the normalization pointed out above.

In the ultra-relativistic limit, $m_0c^2 << \varepsilon_{F0} \approx \varepsilon_{F0}$, the Sagdeev potential reduces to

$$V_U(\Phi_U) = -\frac{1}{3\left(1+\frac{\pi^2 T_U^2}{3}\right)} \left\{ \left(1+\pi^2 T_U^2\right)\Phi_U + \frac{3}{2}\left(1+\pi^2 T_U^2/3\right)\Phi_U^2 + \Phi_U^3 + \frac{\Phi_U^4}{4} + 2M_U^2\left(1+\pi^2 T_U^2\right)\left(1-\frac{\Phi_U}{M_U^2}\right)^{1/2} - 2M_U^2\left(1+\pi^2 T_U^2\right) \right\} \tag{33}$$

$$\mathscr{M}_{U,\text{low}} = \frac{1}{A_U}\sqrt{\frac{1}{6}\left(\frac{1+\pi^2 T_U^2}{1+\pi^2 T_U^2/6}\right)}. \tag{34}$$

We note that in both the limiting cases, the expressions for the Sagdeev potentials are less complicated by comparison with the general relativistic case.

3.4 Results and discussion

In this section, we numerically investigate our results by applying the conditions present on white dwarfs. Although conditions on white dwarfs are such that there is a whole range of magnetic field and number density values, we choose $n = 10^{26}$–10^{29} cm^3 and $n = 10^{30}$–10^{32} cm^3 (Koester and Chanmugam 1990) for non-relativistic, and relativistic and ultra-relativistic cases, respectively. First, we consider the Sagdeev potential for the relativistic case given by Eq. (30) plotted in Fig. 1. Figure 1 (upper panel) shows the Sagdeev potentials for different values of electron temperature T. We can note that with the increases in temperature, the Sagdeev potential depth as well as maximum value of Φ increases. Soliton profiles corresponding to the Sagdeev potentials are plotted in Fig. 1 (lower panel), in which we can see that amplitude as well as width of soliton increases with the increase in temperature T.

Figure 2 (upper panel) shows the Sagdeev potentials for different values of relativistic energy, ε_0. We can note that with the increases in relativistic energy, the Sagdeev potential depth as well as maximum value of Φ decreases. Soliton profiles corresponding to the Sagdeev potentials are plotted in Fig. 2 (lower panel), in which we can see that amplitude as well as width of soliton decreases with the increase in relativistic energy ε_0.

Similarly, Fig. 3 shows the variation in Mach number. Figure 3 (upper panel) shows the Sagdeev potentials for different values of Mach number. It can be seen that Sagdeev potential shows greater sensitivity with the Mach number as compared to Figs. 1 and 2. We can see that with the increases in Mach number, Sagdeev potential depth as well as maximum value of Φ increases. Soliton profiles corresponding to the Sagdeev potentials are plotted in Fig. 3 (lower panel), in which we can see that amplitude increases but width of soliton decreases with the increase in Mach number.

Figure 4 depicts that when the normalized electron temperature is larger than a certain value, i.e. $T_R \geq 0.3$ for this particular case, we obtain both compressive and rarefactive solitons, similar to one of our papers (Shah et al. 2010). We can see that

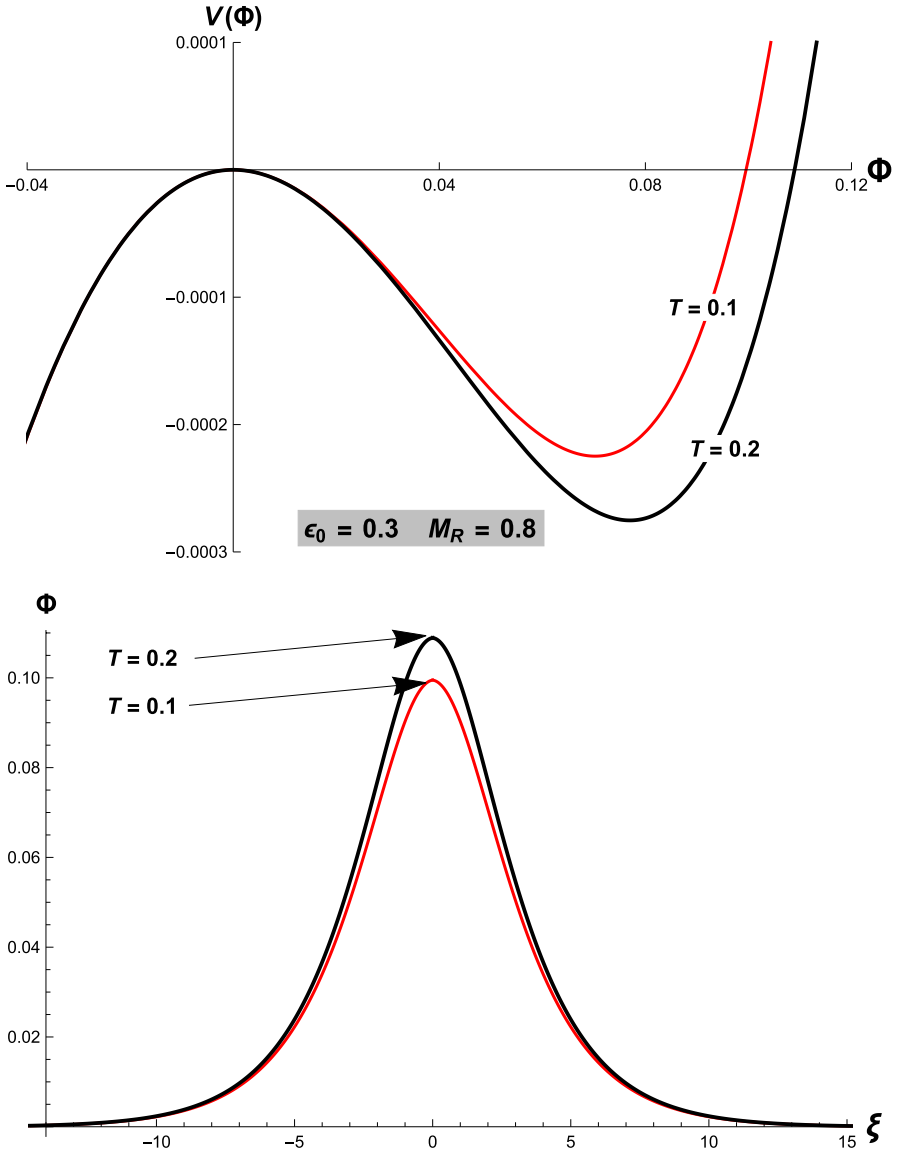

Fig. 1 Sagdeev potential (upper panel) and corresponding solitary structures (lower panel) for different values of T for fixed values of $\varepsilon_0 = 0.3$ and $M_R = 0.8$

with the increase in temperature, amplitude of compressive soliton increases but width decreases slightly,: however, for the rarefactive solitons amplitude decreases but width increases slightly as shown in Fig. 4 (lower panel).

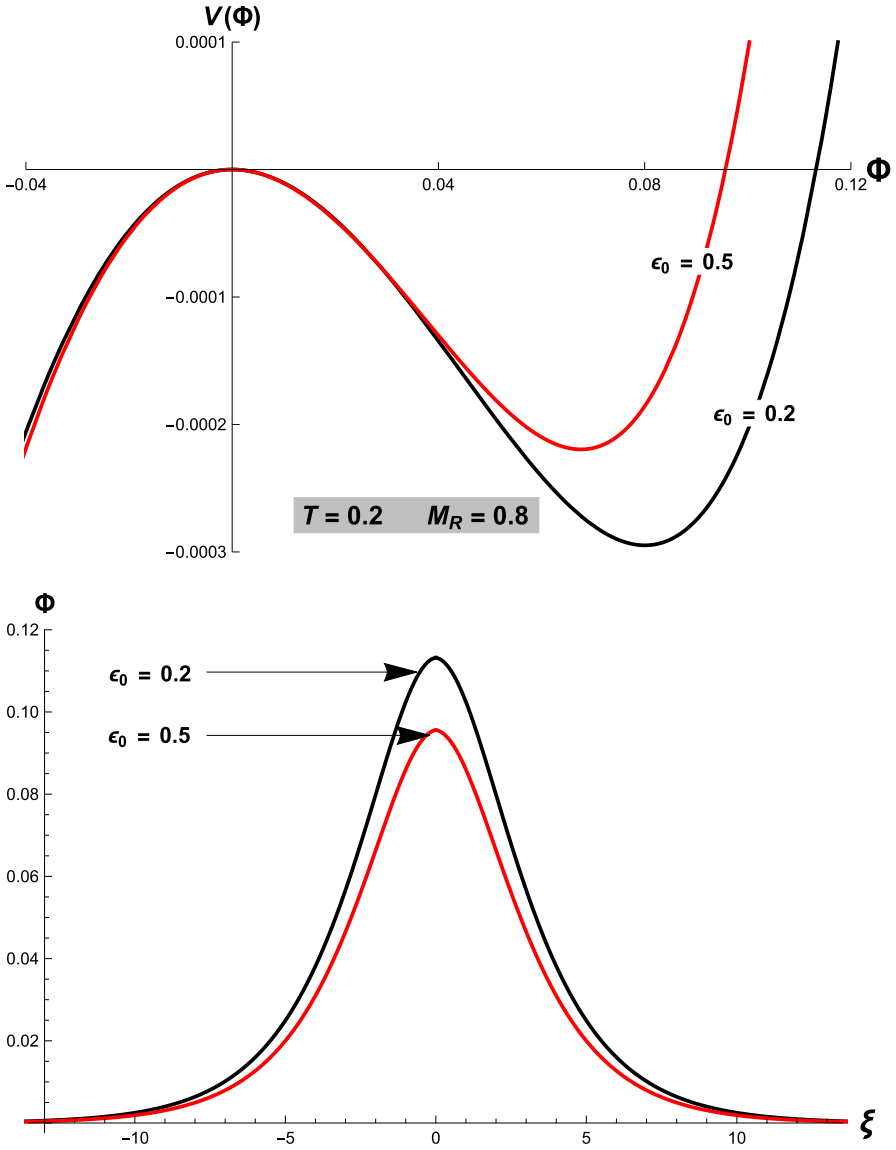

Fig. 2 Sagdeev potential (upper panel) and corresponding solitary structures (lower panel) for different values of ε_0 for fixed values of $T = 0.2$ and $M_R = 0.8$

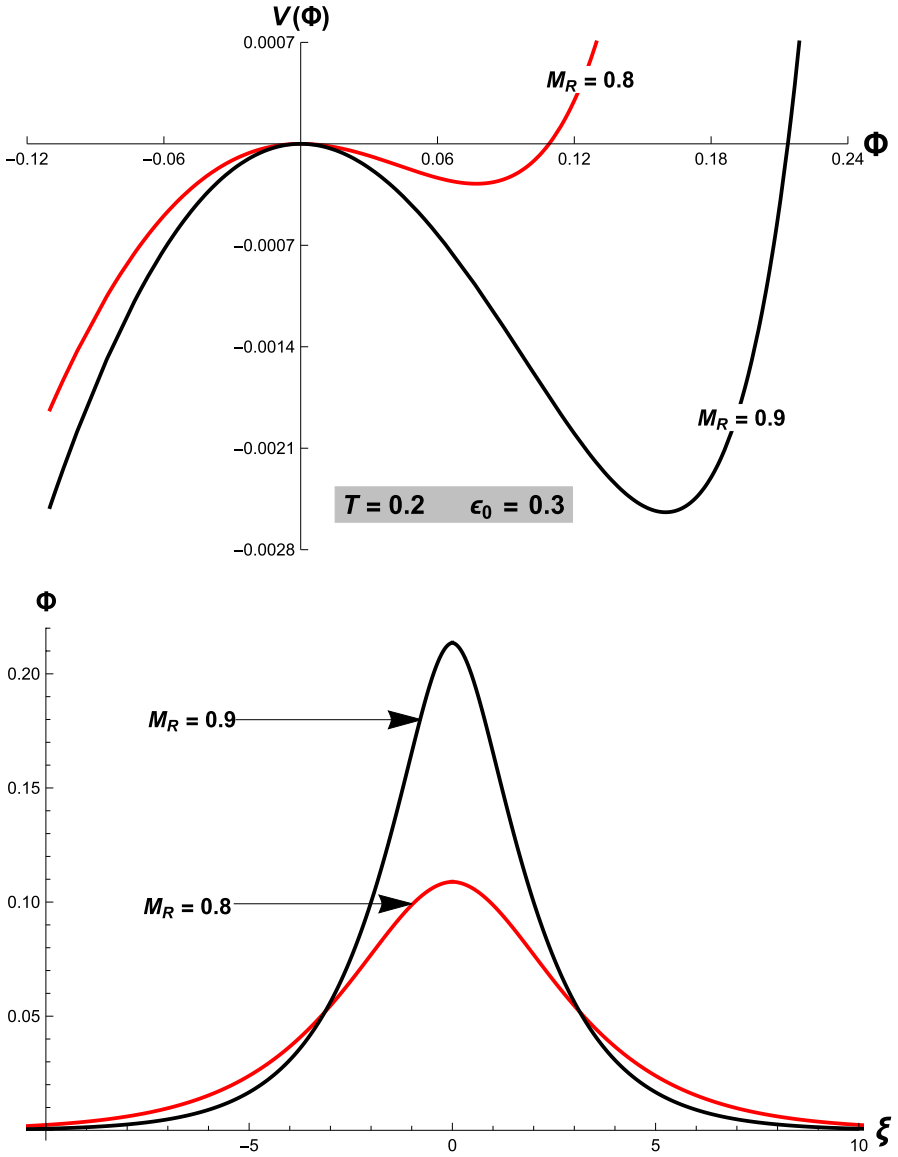

Fig. 3 Sagdeev potential (upper panel) and corresponding solitary structures (lower panel) for different values of M_R for fixed values of $T = 0.2$ and $\varepsilon_0 = 0.3$

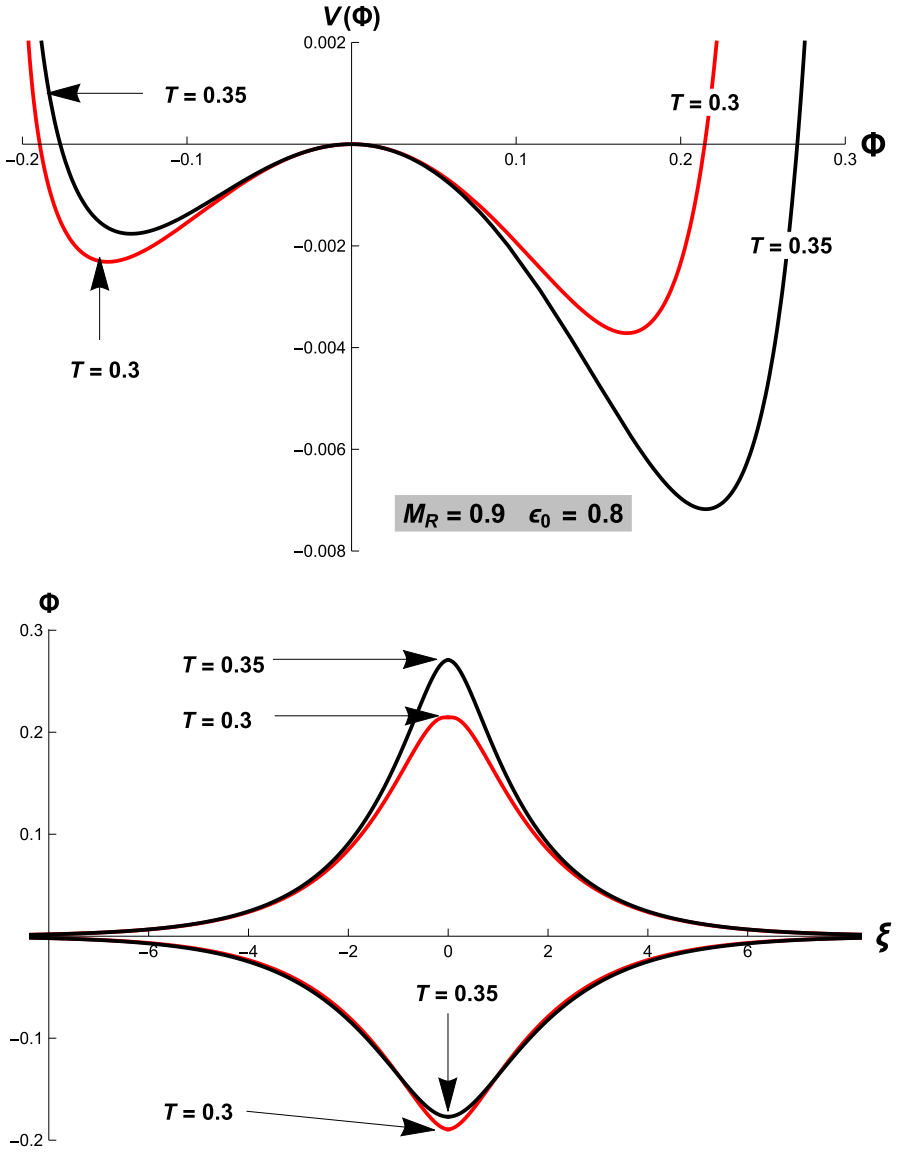

Fig. 4 Asymmetric Sagdeev potential (upper panel) and corresponding solitary structures (lower panel) for different values of T for fixed values of $M_{\mathrm{R}} = 0.9$ and $\varepsilon_0 = 0.8$

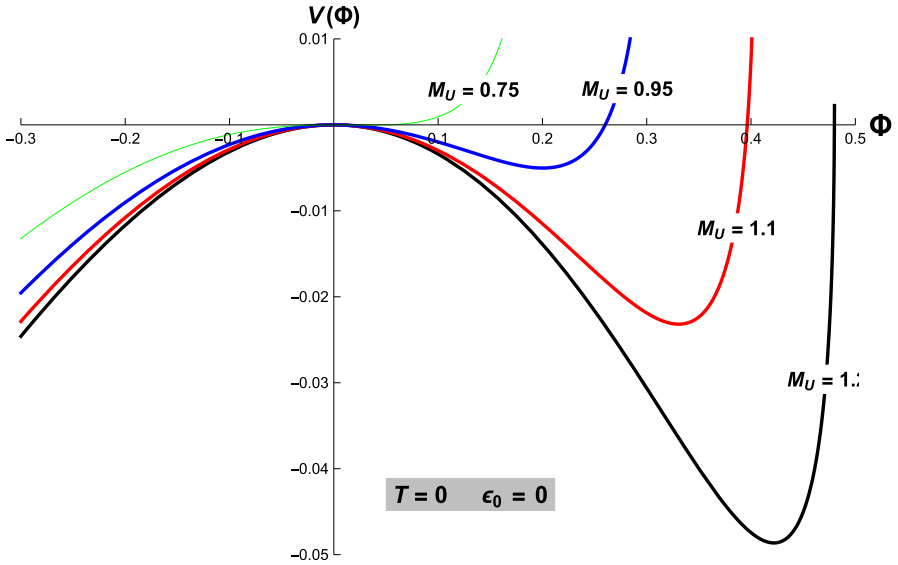

Fig. 5 Sagdeev potential for different values of M_{U} when $T = 0$ and in the ultrarelativistic limit, i.e. $\epsilon_0 = 0$

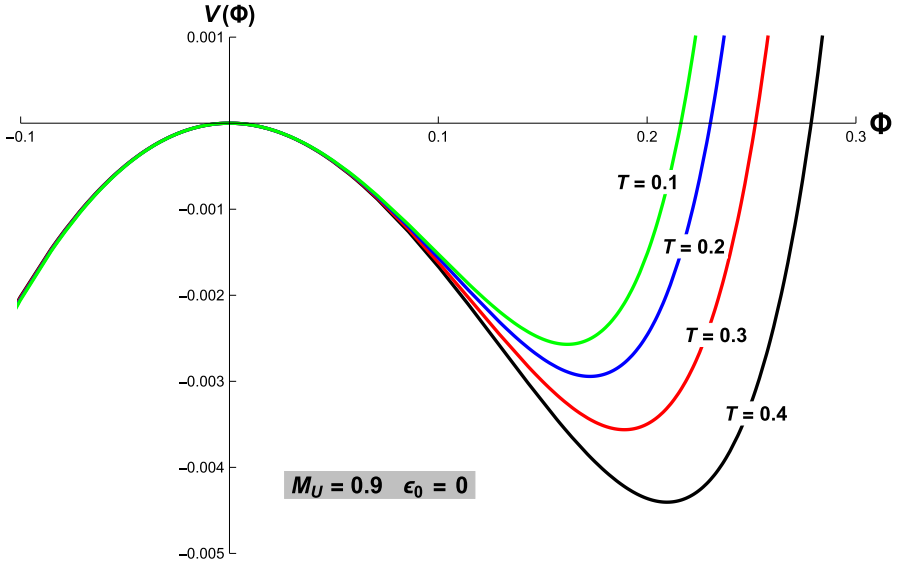

Fig. 6 Sagdeev potential for different values of T for $M_{\mathrm{U}} = 0.9$ and in the ultrarelativistic limit, i.e. $\epsilon_0 = 0$

We now consider the ultra-relativistic case for which we have plotted the Sagdeev potential for different values of ultra-relativistic Mach number M_U in Fig. 5. It is observed that when we increase the ultra-relativistic Mach number, the depth as well as the maximum value of potential decreases appreciably. Figure 6 depicts the Sagdeev potential when the finite electron temperature has been included for the ultra-relativistic. It can be observed that as temperature increases the width as well as maximum value of potential increases. Finally, we would like to mention that the soliton amplitude has been found to be largest for non-relativistic, intermediate for ultra-relativistic, and least for the relativistic case.

4 Landau quantization

In this section, we review our work on nonlinear IAWs for adiabatic trapping (Shah et al. 2012; Iqbal et al. 2017) in a plasma where the electrons are Landau quantized. We adopt the same procedure here as outlined in Sect. 2 to obtain the expression of electron number density. The motion of electrons are Landau quantized in a strong magnetic field (Wahab and Solid, 2005) which occurs in the plane perpendicular to the magnetic field. The total energy at different levels ℓ in the non-relativistic limit in the presence of a potential field φ given by Wahab (2005)

$$\varepsilon_e^{\ell} = \ell \hbar \omega_{\mathrm{ce}} + \frac{p_z^2}{2m_{\mathrm{e}}} - e\varphi, \tag{35}$$

where $\omega_{ce} = eB_0/m_e c$ is the electron gyrofrequency, $-e\varphi$ is the potential energy of the well in which the electrons are trapped and p_z is the parallel electron momentum. The external magnetic field $\boldsymbol{B}_0 = \hat{z}B_0$ is in the $\hat{z}$ direction. Electron capture takes place when $\varepsilon_e^{\ell} = 0$ holds.

The total occupation number for the Fermi–Dirac distribution after in tegration over the polar coordinates gives (Landau and Lifshitz 1980)

$$n_{\mathrm{e}} = \frac{p_{\mathrm{Fe}}^2 \eta}{2\pi^2 \hbar^3} \sqrt{\frac{m_{\mathrm{e}}}{2}} \sum_{\ell=0}^{\varepsilon} \int_0^{\varepsilon} \frac{\varepsilon^{-1/2}}{\exp\left\{\frac{\varepsilon - U}{\mathrm{T}}\right\} + 1} \mathrm{d}\varepsilon, \tag{36}$$

where $U = e\varphi + \mu - \ell\hbar\omega_{\mathrm{ce}}$, The quantizing magnetic field manifests itself through $\eta = \hbar\omega_{\mathrm{ce}}/\varepsilon_{\mathrm{Fe}}$. The unquantized case is represented by $\ell = 0$. In most macroscopic systems, eigenvalue spectrum for energy is of a very high density of energy, thus $\ell \gg 1$, whereas the energy spectrum (in a finite range) exhibits an exponential enhancement in a finite range of energy spectrum with the increasing number of particles N in the system. It is found that the separation between the levels is proportional to 10^{-N} (Tsintsadze 2010). We have, therefore, considered a continuous energy spectrum—which is a reasonable assumption. Consequently, to arrive at an expression of the density, n_{e}, we can separate the $\ell = 0$ case and replace the summation in Eq. (36) by integration ($\sum_1^{\ell_{\max}} \to \int_1^{\ell_{\max}} \mathrm{d}\ell$), where $\ell_{\max} = (1 + \frac{e\varphi}{\varepsilon_{\mathrm{Fe}}})/\eta$ which we get

by requiring the integrand to be a real quantity. Adopting the procedure as outlined in Sect. 2, we obtain the expression for the total number density as follows:

$$n_{\mathrm{e}} = N_0\left[\frac{3}{2}\eta(1+\Phi)^{\frac{1}{2}} + (1+\Phi-\eta)^{3/2} - \frac{\eta T^2}{2}(1+\Phi)^{-\frac{3}{2}} + T^2(1+\Phi-\eta)^{-1/2}\right]. \tag{37}$$

For a fully degenerate plasma, the background number density is given by $N_0 = p_{\mathrm{Fe}}^3/3\pi^2\hbar^3$. The limit $\eta = 0$, yields the results reported in Ref. Shah et al. (2010). Note that the role of parameter η is akin to the finite temperature T corrections in altering the occupation number density of electrons n_{e}. As mentioned in the previous sections when $T/\varepsilon_{\mathrm{Fe}} \ll 1$, assuming $\mu = \varepsilon_{\mathrm{Fe}}$ is reasonable. The normalization is done as follows: $T = \pi T/2\sqrt{2}\varepsilon_{\mathrm{Fe}}$ and $\Phi = e\varphi/\varepsilon_{\mathrm{Fe}}$.

Next, we focus ourselves on the ions which are considered cold and classical due to their inertia. The ion momentum equation is given by

$$\left[\frac{\partial\vec{v}_i}{\partial t} + \left(\vec{v}_i\cdot\vec{\nabla}\right)\vec{v}_i\right] = -\frac{e}{m_i}\vec{\nabla}\varphi + \frac{e}{m_i}\left(\vec{v}_i\times\vec{B}\right). \tag{38}$$

The above equation is supplemented by the continuity and Poisson's equations (see Sect. 3). Assuming sinusoidal perturbation in the above set of equations, we obtain the following linear dispersion relation for IAWs in the presence of Landau quantization and small temperature corrections:

$$\frac{\omega}{k} = C_{\mathrm{sF}}\left[\frac{2\left\{\left(3-T^2\right)\frac{\eta}{2} + (1-\eta)^{3/2} + T^2(1-\eta)^{-1/2}\right\}}{\left(1+T^2\right)\frac{3\eta}{2} + 3(1-\eta)^{1/2} - T^2(1-\eta)^{-3/2} + 2k^2\lambda_{\mathrm{TF}}^2}\right]^{1/2}, \tag{39}$$

where C_{sF} and λ_{TF} are the acoustic speed and screening length in Fermi plasmas as given in the preceding section. Following the procedure elucidated in Sect. 2, we find the following expression of the nonlinear ion number density:

$$n_i = N_0\left[\left(3-T^2\right)\frac{\eta}{2} + (1-\eta)^{\frac{3}{2}} + T^2(1-\eta)^{-\frac{1}{2}}\right]\left(1-\frac{2\Phi}{M^2\alpha}\right)^{-1/2}, \tag{40}$$

$M = \frac{u}{\omega/k}$ is the Mach number and

$$\alpha = \frac{2\left\{\left(3-T^2\right)\frac{\eta}{2} + (1-\eta)^{3/2} + T^2(1-\eta)^{-1/2}\right\}}{\left(1+T^2\right)\frac{3\eta}{2} + 3(1-\eta)^{1/2} - T^2(1-\eta)^{-3/2}}.$$

4.1 Sagdeev potential

To obtain an expression for the Sagdeev potential and investigate the presence of solitary waves, we substitute the values of n_e and n_i from Eqs. (37) and (40) in the Poisson's equation and arrive at the following expression:

$$\frac{\mathrm{d}^2\Phi}{\mathrm{d}\xi^2} = \Bigg[\Bigg\{\frac{3}{2}\eta(1+\Phi)^{\frac{1}{2}} + (1+\Phi-\eta)^{\frac{3}{2}} - \frac{\eta T^2}{2}(1+\Phi)^{-\frac{3}{2}} + T^2(1+\Phi-\eta)^{-1/2} - \Bigg\{\big(3-T^2\big)\frac{\eta}{2} + (1-\eta)^{\frac{3}{2}} + T^2(1-\eta)^{-\frac{1}{2}}\Bigg\}\Big(1-\frac{2\Phi}{M^2\alpha}\Big)^{-1/2}\Bigg], \tag{41}$$

where ξ is normalized as $\xi = \xi/\lambda_{\mathrm{TF}}$. Equation (41) can be expressed in the form of an energy integral as was shown in Eq. (29) and we can obtain the Sagdeev potential which now has the form

$$\begin{aligned} V(\Phi) = &\Big[\big(1+T^2\big)\eta + \frac{2}{5}(1-\eta)^{5/2} - \eta(1+\Phi)^{3/2} - \frac{2}{5}(1+\Phi-\eta)^{5/2} \\ &+M^2\alpha\beta - M^2\alpha\beta\Big(1-\frac{2\Phi}{M^2\alpha}\Big)^{1/2} - \eta T^2(1+\Phi)^{-1/2} \\ &- 2T^2(1+\Phi-\eta)^{1/2} + 2T^2(1-\eta)^{1/2}\Big]. \end{aligned} \tag{42}$$

Here

$$\beta = \big(3-T^2\big)\frac{\eta}{2} + (1-\eta)^{3/2} + T^2(1-\eta)^{-1/2}.$$

Upon the fulfillment of the conditions given in Ref. Mamun (1997), compressive and rarefactive solitary waves are obtained.

We obtain the lower bound of the Mach number from Eq. (42) by Taylor expanding the coefficients and setting the square order terms in Φ equal to zero as follows:

$$M \geq 1$$

Similarly, we obtain the upper bound of Mach number is obtained from Eq. (42) using the requirement that the expression should remain real valued. Thus, the upper limit is given by

$$M < \left\{\frac{\big(1+T^2\big)\frac{3\eta}{2} + 3(1-\eta)^{1/2} - T^2(1-\eta)^{-3/2}}{\big(3-T^2\big)\frac{\eta}{2} + (1-\eta)^{3/2} + T^2(1-\eta)^{-1/2}}\right\}^{1/2}.$$

We, therefore, get the following range of M:

$$1 \leq M < \left\{\frac{\big(1+T^2\big)\frac{3\eta}{2} + 3(1-\eta)^{\frac{1}{2}} - T^2(1-\eta)^{-\frac{3}{2}}}{\big(3-T^2\big)\frac{\eta}{2} + (1-\eta)^{\frac{3}{2}} + T^2(1-\eta)^{-\frac{1}{2}}}\right\}^{\frac{1}{2}}. \tag{43}$$

Now, we discuss the limiting cases. We note that when $\eta = 0$, the Sagdeev potential reduces to

$$V(\Phi) = \left[\frac{2}{5} - \frac{2}{5}(1+\Phi)^{\frac{5}{2}} + M^2\alpha\beta - M^2\alpha\beta\Big(1-\frac{2\Phi}{M^2\alpha}\Big)^{\frac{1}{2}} + 2T^2 - 2T^2(1+\Phi)^{\frac{1}{2}}\right], \tag{44}$$

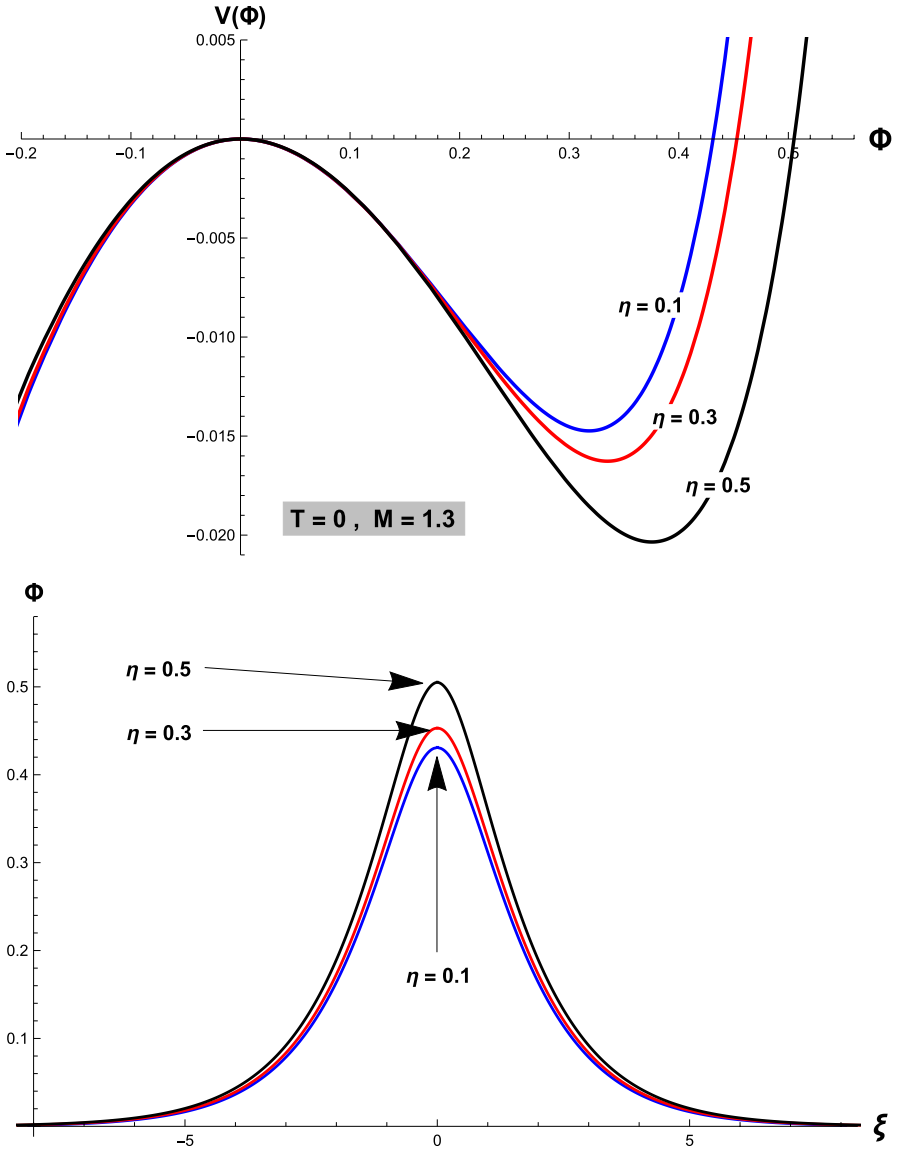

Fig. 7 Sagdeev potential (upper panel) and corresponding solitary structures (lower panel) for different values of η when $T = 0$ and $M = 1.3$

where $\alpha = \frac{2(1+T^2)}{3-T^2}$ and $\beta = 1 + T^2$ and the range of Mach number is given by

$$1 \leq M < \left\{ \frac{3 - T^2}{1 + T^2} \right\}^{\frac{1}{2}},$$

which is the same result we obtained in Ref. Shah et al. (2010).

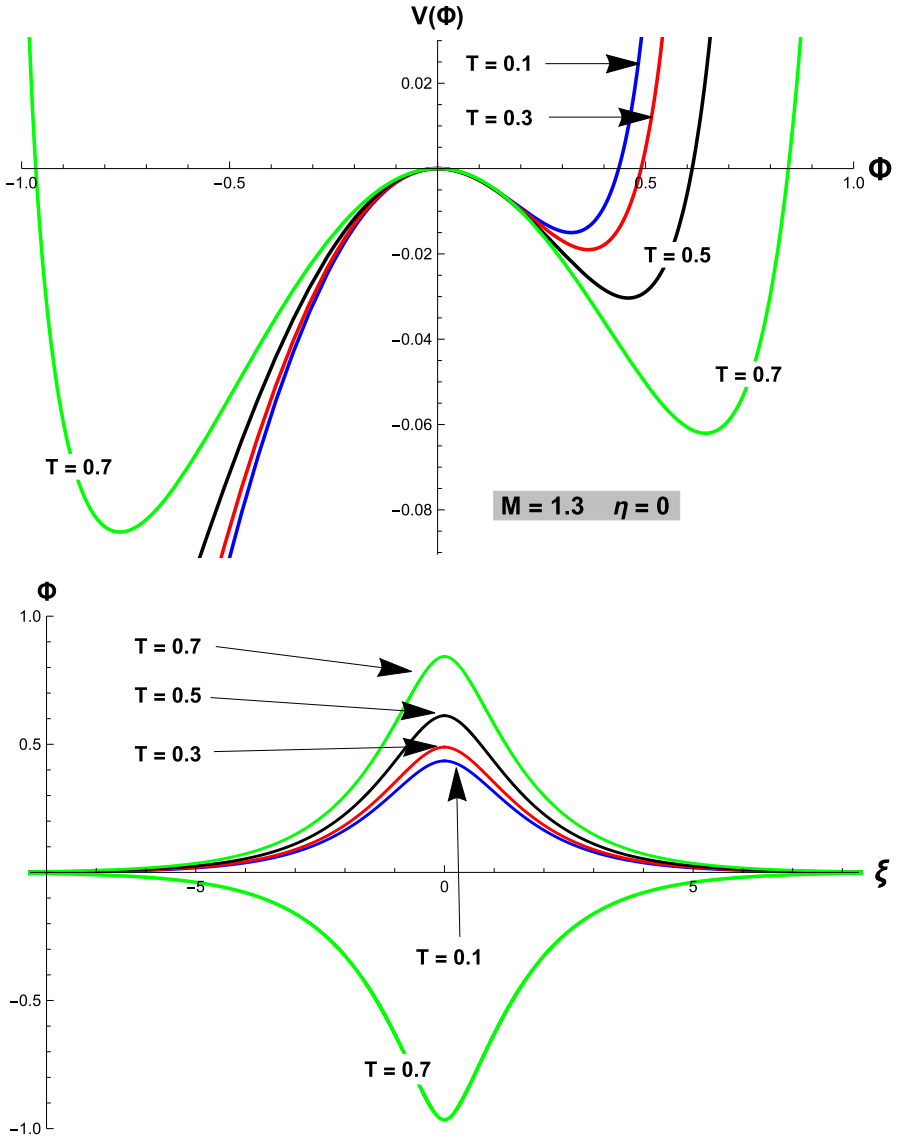

Fig. 8 Sagdeev potential (upper panel) and corresponding solitary structures (lower panel) for different values of T when $\eta = 0$ and $M = 1.3$

4.2 Results and discussion

In the present section, we will numerically investigate the results obtained in Sect. 4.1 by plotting the Sagdeev potential and see how these are affected by varying different parameters such as magnetic field (η), temperature (T) and Mach

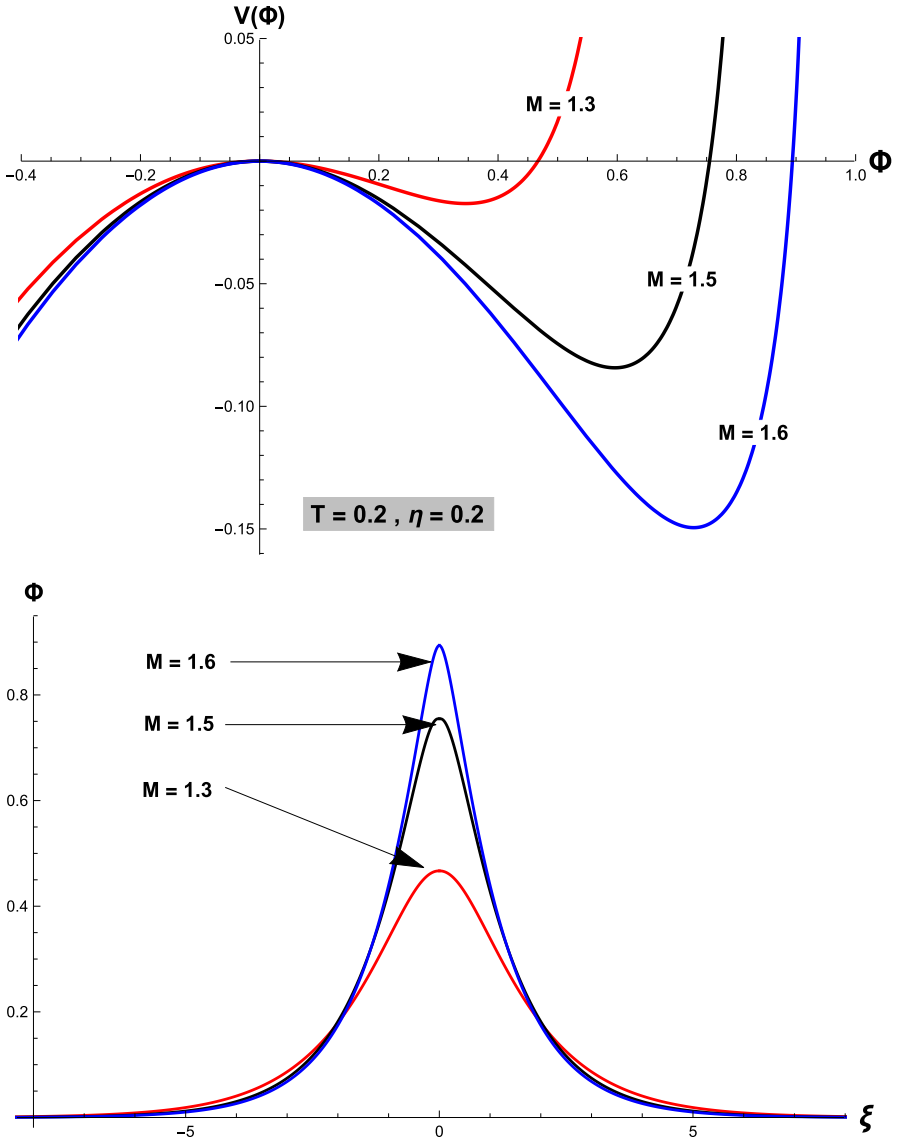

Fig. 9 Sagdeev potential (upper panel) and corresponding solitary structures (lower panel) for different values of M when $\eta = 0.2$ and $T = 0.2$

number (M). For the numerical purposes we take the values of magnetic field and number density as 10^{10}G and 10^{26}cm^{-3}, respectively, which are typical values found for the white dwarfs (Shah et al. 2011; Koester and Chanmugam 1990). The Fermi temperature is calculated as $T_{\mathrm{Fe}} = 9.14108 \times 10^{6}$K by calculating the

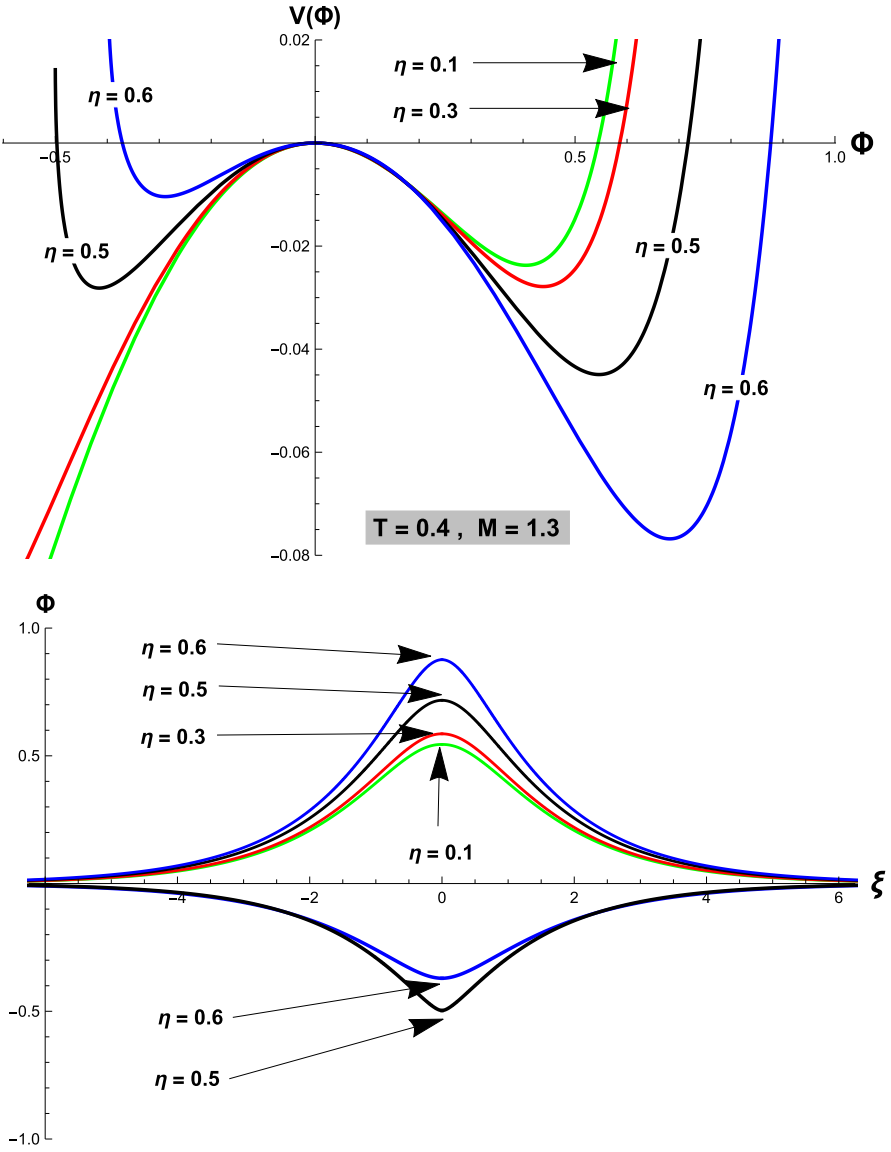

Fig. 10 Sagdeev potential (upper panel) and corresponding solitary structures (lower panel) for different values of η when $T = 0.4$ and $M = 1.3$

Fermi energy using the value of number density given above and also the electron temperature is considered as $T \ll T_{\mathrm{Fe}}$.

Figure 7 depicts the plots for fully degenerate plasma, i.e., $T = 0$ using Eq. (42). In Fig. 7 (upper panel) Sagdeev potentials are plotted for different magnetic field strengths, η. It can be noted that the depth as well as the maximum value of potential increases with the increase in η. In Fig. 7 (lower panel) the

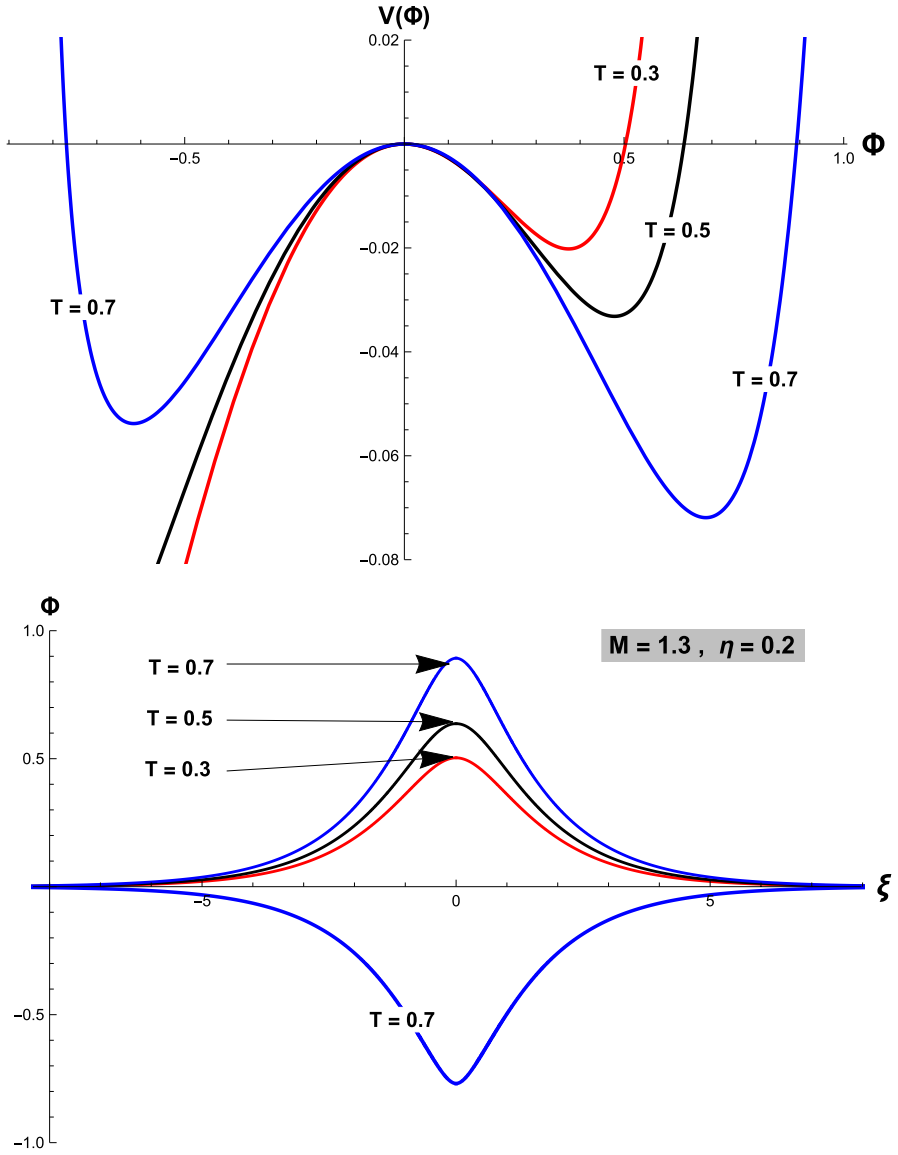

Fig. 11 Sagdeev potential (upper panel) and corresponding solitary structures (lower panel) for different values of T when $\eta = 0.2$ and $M = 1.3$

corresponding solitons are plotted whose width and amplitude increases with the increase in η. It should be mentioned here that only compressive structures can be obtained for fully degenerate plasma, i.e., $T = 0$.

Figure 8 shows the plots in which we ignore the magnetic field effect, i.e. $\eta = 0$ but we consider $T \neq 0$ using Eq. (42). In Fig. 8 (upper panel) Sagdeev potentials are plotted for different electron temperatures. We can see that when we increase the

temperature not only the width and maximum value of potential increases but for $T \geq 0.6$ we obtain two values of potential Φ_{min} and Φ_{max}. Corresponding solitons are plotted in Fig. 8 (lower panel) in which we can see that amplitude of compressive solitons increases but rarefactive solitons decreases with the increase in temperature. The same effect has been reported in Ref. Mamun (1997) and such coupled (compressive and rarefactive) solitary structures are observed in space plasmas (Ghosh and Lakhina 2004).

Figure 9 (upper panel) shows Sagdeev potentials for different values of Mach number M. It can be seen that the depth as well as the maximum value of potential increases with the increase in M. In Fig. 9 (lower panel) the corresponding solitons are plotted whose amplitude increases but width decreases with the increase in M. Figure 10 shows the plots for different values of magnetic field strength η. In Fig. 10 (upper panel) Sagdeev potentials are plotted for different values of η in which we can see that when we increase the value of $\eta > 0.4$, we obtain two values of potential Φ_{min} and Φ_{max}. It can also be seen that the width and maximum value of compressive Sagdeev potentials increase but rarefactive Sagdeev potentials decrease with the increase in η. Corresponding solitons are plotted in Fig. 10 (lower panel) in which we can see that amplitude of compressive solitons increases but rarefactive solitons decreases with the increase in η. Similarly, Fig. 11 shows the plots for different values of temperature T but $\eta \neq 0$. In Fig. 11 (upper panel) Sagdeev potentials are plotted for different values of T in which we can see that when we increase the value of $T \geq 0.6$, we obtain two values of potential Φ_{min} and Φ_{max}. It can also be seen that the width and maximum value of compressive Sagdeev potentials increase with the increase in T. Corresponding solitons are plotted in Fig. 11 (lower panel) in which we can see that amplitude of compressive solitons increases with the increase in T.

5 Drift and drift ion acoustic waves

In this section, we consider the effect of adiabatic trapping of electrons in an inhomogeneous dense quantum plasma and review the results of our work on drift waves (Shah et al. 2014) and our work on drift ion acoustic waves (Fayyaz et al. 2020a).

We consider a magnetoplasma comprising cold dynamical ions and trapped Fermi electrons in which the magnetic field $\boldsymbol{B_0}$ is directed along the z-direction and the spatial nonuniformity of background ion density is in the x-direction, i.e., $n_0(x)$. The propagation regime of the wave is assumed to be $v_{Fe} \gg \omega/k \gg v_{Fi}$, where $v_{Fe,Fi} = \hbar^2/m_{e,i}(3\pi^2 n_0)^{1/3}$ are the Fermi velocities of electrons and ions. The ions are considered to be classical due to reasons mentioned in the previous sections. Using the ion momentum equation (Eq. (38)) along with the ion continuity equation and Poisson's equation and further by invoking the drift wave approximation (Weiland 1999) in the low wave frequency limit ($\Omega_{ci} \gg \partial_t$), the components of ion velocity in the parallel and perpendicular directions read as

$$\hat{L} v_{iz} = -\frac{e}{m_i} \partial_z \varphi \tag{45}$$

$$v_{i\perp} = \frac{c}{B_o}(\hat{z} \times \nabla\varphi) - \frac{c}{B_o \Omega_{ci}} \partial_t \nabla_\perp \varphi, \tag{46}$$

where $\widehat{L} = \partial_t + \boldsymbol{v_E}.\nabla_\perp + v_{iz}\partial_z$ and $\Omega_{ci} = eB_o/\mathrm{cm_i}$ is the ion Larmor frequency and $\boldsymbol{v_{i\perp}}$ contains the $\mathbf{E}\times\mathbf{B}$ and the polarization drifts, respectively. We have used Eq. (5) or Ref. Shah et al. (2010) that gives an expression for the electron number density in the presence of adiabatic trapping in quantum plasmas, bearing in mind that n_o is a function of space. From Eq. (5) and Poisson's equation, the total number density of the ions in the case of a fully degenerate plasma reads as

$$n_i = -\frac{1}{4\pi e}\nabla^2\varphi + n_o\left(1 + \frac{e\varphi}{\varepsilon_F}\right)^{3/2}. \tag{47}$$

Further, by using the ion continuity equation and imposing the order $\partial_y > \partial_z > \partial_x$, we obtain the following expression that represents the coupling of drift and acoustic modes in the presence of quantum trapping of electrons:

$$\begin{aligned} \partial_t^2(1+\Phi)^{3/2} - \lambda_{Fe}^2\partial_t^2\left(\partial_y^2 + \partial_z^2\right)(1+\Phi) - \rho_i^2\partial_t^2\partial_y^2(1+\Phi) \\ + \frac{3}{2}v_*\partial_y\partial_t(1+\Phi) - c_s^2\partial_z^2(1+\Phi) = 0. \end{aligned} \tag{48}$$

Here $\rho_i = c_s/\Omega_{ci}$ is the ion Larmor radius, $v_* = \left(-2c\varepsilon_F/3eB_o\right)\kappa$ is the drift velocity and $\kappa = \left|d_x \ln n_0\right|$ represents the reciprocal of the scale length of inhomogeneity. Equation (48) is the new equation representing the coupling of drift and acoustic modes in a fully degenerate plasma with the inclusion of quantum trapping of electrons. We note here that if $\partial_z = 0$, then we retrieve the results of our earlier paper on drift waves (Shah et al. 2014).

Assuming plane wave solution, we obtain the following linear dispersion relation from Eq. (48) for two-dimensional drift acoustic mode in the presence of quantum trapping of electrons

$$\omega = \frac{1}{2\gamma}\left[\omega_* \pm \left(\omega_*^2 + \frac{8}{3}c_s^2k_z^2\gamma\right)^{1/2}\right], \tag{49}$$

where $\gamma = 1 + 2/3\left\{(\lambda_{Fe}^2 + \rho_i^2)k_y^2 + \lambda_{Fe}^2k_z^2\right\}$, $\omega_* = v_*k_y$ is the drift frequency, $k_y = k\cos\theta$, $k_z = k\sin\theta$ are the wave numbers and θ is the angle between the propagation vector k and y-axis. The factor 8/3 is a result of the trapping term $(1+\Phi)^{3/2}$. Ignoring the spatial inhomogeneity (or $k_y \to 0$) gives the pure ion sound wave, i.e., $\omega = \sqrt{2/3}c_sk_z\Big/\sqrt{1 + 2/3\lambda_{Fe}^2k_z^2}$ and drift wave (Shah et al. 2014), i.e., $\omega = \omega_*\Big/1 + 2/3\left\{(\lambda_{Fe}^2 + \rho_i^2)k_y^2\right\}$ for $k_z \to 0$ in fully degenerate plasmas.

5.1 New model equation with fractional nonlinearity

Equation (48) describes the nonlinear evolution of the drift ion acoustic wave with the inclusion of adiabatically trapped degenerate electrons. We employ the Sagdeev potential approach to analyze the equation. This equation is transformed by using a co-moving frame $\xi = k_y y + k_z z - \Omega t$ where q_y and q_z are the nonlinear wave numbers and Ω is the frequency of nonlinear structure. This transformation yields

$$\frac{\mathrm{d}}{\mathrm{d}\xi}\left\{\frac{\mathrm{d}}{\mathrm{d}\xi}(1+\Phi)^{3/2} - A\frac{\mathrm{d}^3}{\mathrm{d}\xi^3}(1+\Phi)\right\} - B\frac{\mathrm{d}^2}{\mathrm{d}\xi^2}(1+\Phi) = 0, \tag{50}$$

where $A = \left\{(\lambda_{\mathrm{Fe}}^2 + \rho_i^2)k_y^2 + \lambda_{\mathrm{Fe}}^2 k_z^2\right\}$ and $B = \left(c_s^2 k_z^2/\Omega^2 + 3\omega_*/2\Omega\right)$. Upon integration and making use of the boundary condition $\Phi \to 0$ as $\xi \to \infty$, we obtain

$$\frac{\mathrm{d}^2(1+\Phi)}{\mathrm{d}\xi^2} = -\frac{\mathrm{d}W(\Phi)}{\mathrm{d}\Phi}. \tag{51}$$

The constants of integration are evaluated by integrating Eq. (12) using the boundary conditions mentioned above which leads to the following Sagdeev potential $W(\Phi)$:

$$W(\Phi) = -\frac{2}{5A}(1+\Phi)^{5/2} + \frac{B}{2A}(1+\Phi)^2 + \frac{(1-B)}{A}(1+\Phi) - \frac{3}{5A} + \frac{B}{2A}. \tag{52}$$

Following the conditions given in Sect. 3 for the formation of a solitary structure, we obtain the permissible range of Mach numbers given here as under

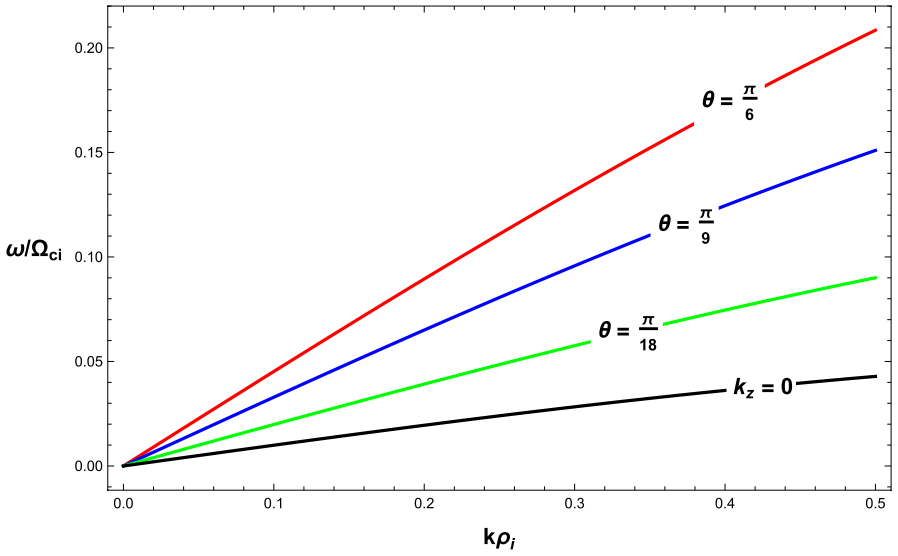

Fig. 12 Linear dispersion relation of ion acoustic wave in inhomogeneous fully degenerate plasma for different values of θ when $n_o = 10^{27}$ cm^{-3} and $B_o = 10^{11}$ G

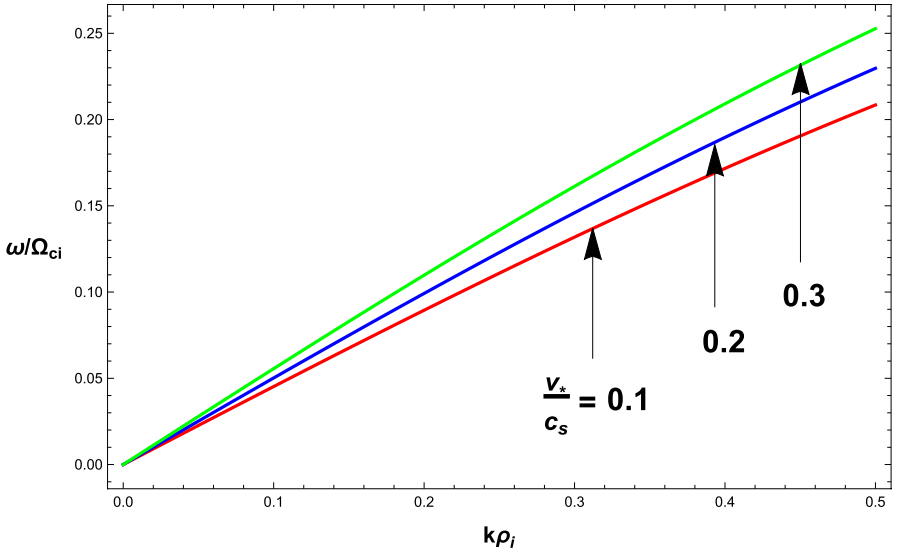

Fig. 13 Linear dispersion relation with the variation in inhomogeneity for different values of v_*/c_s when $n_o = 10^{27}$ cm^{-3} and $B_o = 10^{11}$ G

$$\mathcal{M}_l = \frac{1}{2}\left[\frac{v_* \cos\theta}{c_s} + \sqrt{\frac{v_*^2 \cos^2\theta}{c_s^2} + \frac{8}{3}\sin^2\theta}\right], \tag{53}$$

where $\mathcal{M}_l$ is the lower Mach number. The upper bound of $\mathcal{M}_h$ is obtained by using a physically valid solution, i.e., $\Phi_{\min} \leq -1$ which gives

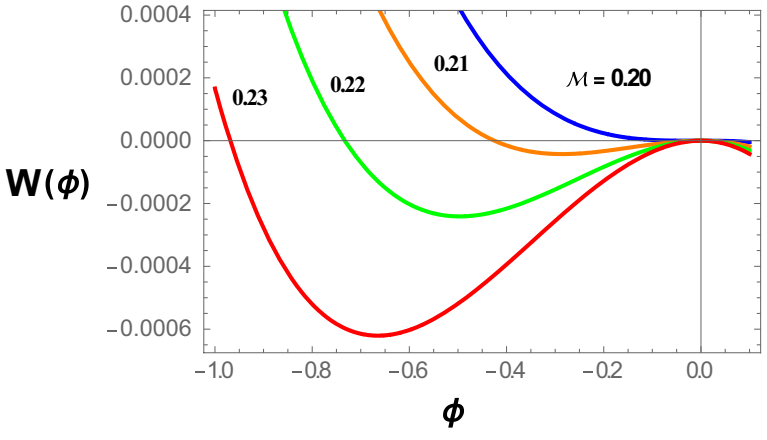

Fig. 14 Sagdeev potentail for different Mach numbers $\mathcal{M}$ when $\theta = \pi/18$ and $v_*/c_s = 0.1$

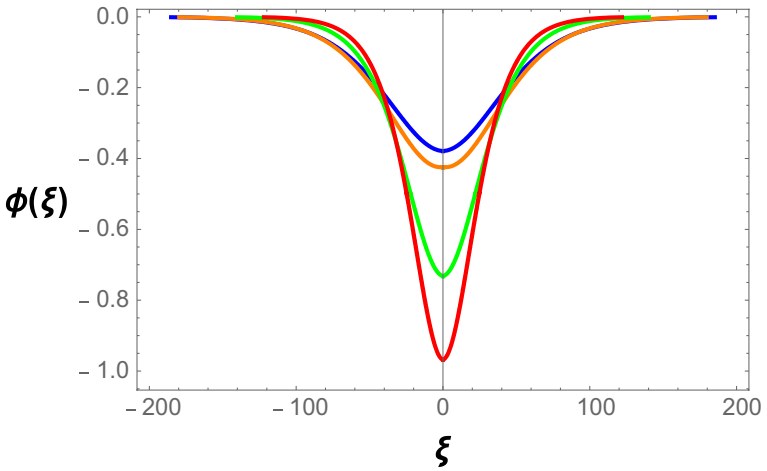

Fig. 15 Rarefactive solitons for different Mach numbers $\mathcal{M} = 0.2$(Blue), 0.21(Orange), 0.22(Green), 0.23(Red) when $\theta = \pi/18$ and ${}^{v_*}/_{c_s} = 0.1$

$$\mathcal{M}_h = \frac{5}{12}\left[\frac{3}{2}\frac{v_*\cos\theta}{c_s} + \sqrt{\frac{9}{4}\frac{v_*^2\cos^2\theta}{c_s^2} + \frac{24}{5}\sin^2\theta}\right]. \tag{54}$$

Equations (53) and (54) clearly show the dependence of the propagation range $\mathcal{M}_l < \mathcal{M} \leq \mathcal{M}_h$ on the drift velocity v_* and the propagation angle θ.

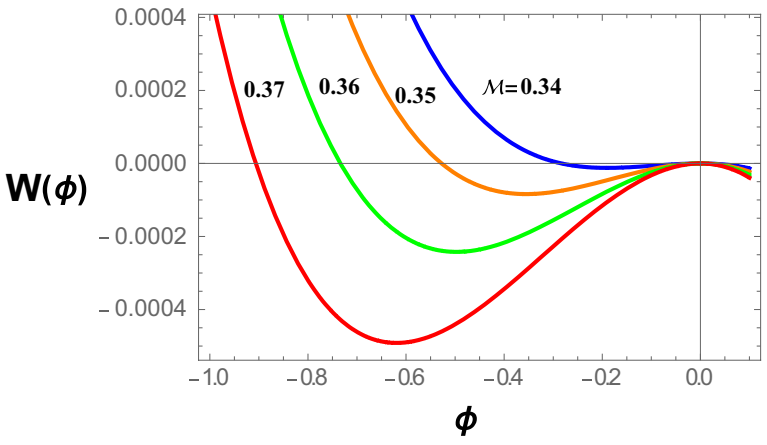

Fig. 16 Sagdeev potentail for different Mach numbers $\mathcal{M}$ when $\theta = \pi/9$ and ${}^{v_*}/_{c_s} = 0.1$

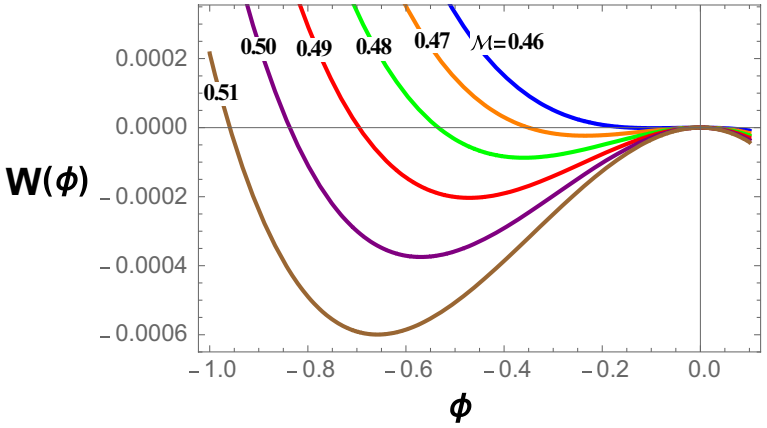

Fig. 17 Sagdeev potentail for different Mach numbers $\mathcal{M}$ when $\theta = \pi/6$ and ${}^{v_*}/_{c_s} = 0.1$

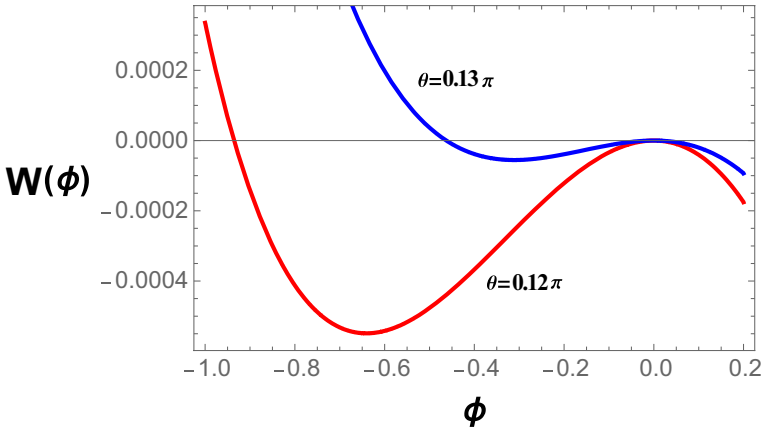

Fig. 18 Sagdeev potentail for different values of θ when $\mathcal{M} = 0.40$ and ${}^{v_*}/_{c_s} = 0.1$

5.2 Results and discussion

In this section, we numerically analyze the positive root of Eq. (49) by considering the numerical values of magnetic field and number density in the ranges $B_o \sim 10^9 - 10^{11}$G and $n_o \sim 10^{26} - 10^{29}\text{cm}^{-3}$, respectively, typically found in neutron stars (Sah and Manta 2009). The density range is chosen to ensure that the electrons remain non-relativistic and degenerate. The other numerical values are considered by following the drift wave conditions ($k_y > k_z$ and $v_* \ll c_s$) so that $c_s = 6 \times 10^7\text{cm/s}$, $\Omega_{ci} = 9.5 \times 10^{14}\text{s}^{-1}$, $v_* = 5.9 \times 10^6\text{cm/s}$ and $\theta \sim \frac{\pi}{18}$ to $\frac{\pi}{6}$ (Shukla and Eliasson 2011). Linear dispersion relation of quantum coupled drift ion acoustic wave is plotted in Fig. 12 for different values of angle of propagation, θ. We can see that the frequency enhances with the wavenumber for the fixed value of

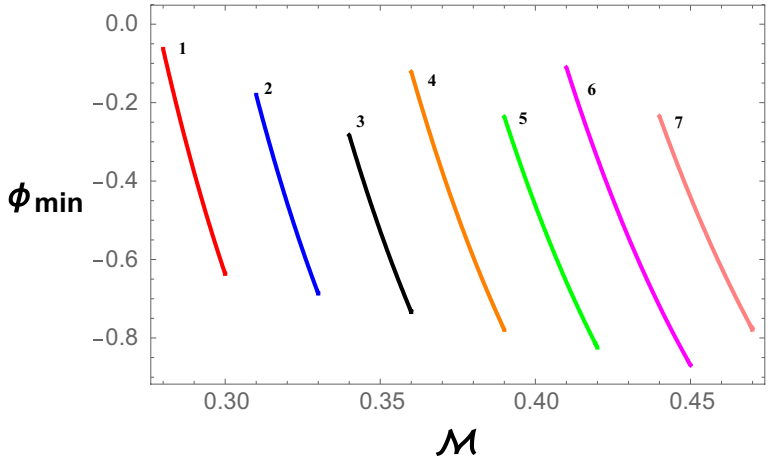

Fig. 19 The amplitude of rarefactive solitons Φ_{min} versus Mach number $\mathcal{M}$ for $^{v_*}/_{c_s} = 0.1$ and different values of θ, i.e. $(1)\theta = 0.08\pi, (2)\theta = 0.10\pi, (3)\theta = 0.12\pi, (4)\theta = 0.14\pi, (5)\theta = 0.16\pi, (6)\theta = 0.18\pi, (7)\theta = 0.20\pi$

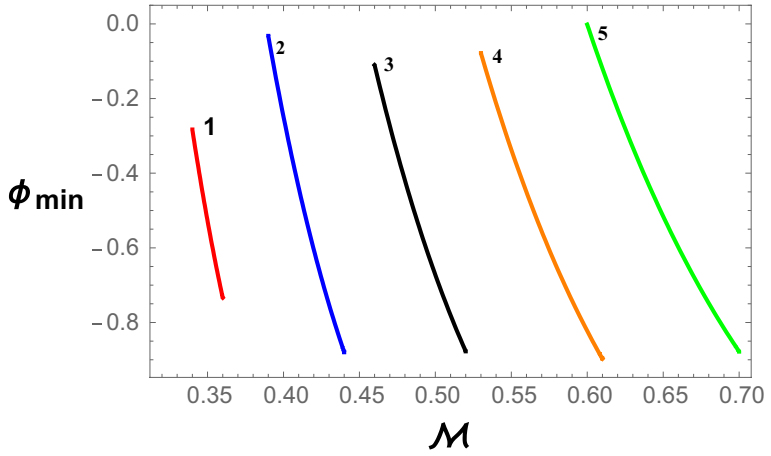

Fig. 20 The amplitude of rarefactive solitons Φ_{min} versus Mach number $\mathcal{M}$ for $\theta = \pi/9$ and different values of $^{v_*}/_{c_s}$, i.e. (1) $^{v_*}/_{c_s} = 0.1$, (2) $^{v_*}/_{c_s} = 0.2$, (3) $^{v_*}/_{c_s} = 0.3$, (4) $^{v_*}/_{c_s} = 0.4$, (5) $^{v_*}/_{c_s} = 0.5$

angle of propagation and increases with the increase in angle of propagation for the fixed value of wavenumber. We also plot the linear dispersion relation of quantum-coupled drift ion acoustic wave for different values of drift velocity v_* in Fig. 13. We can see that the frequency enhances with the increase wavenumber for the fixed value of drift velocity v_* and increases with the increase in drift velocity v_* (or larger inhomogeneity κ) for the fixed value of wavenumber.

Rarefactive Sagdeev potential structures for different Mach numbers are shown in Fig. 14. The Sagdeev potential curves show that as the Mach numbers $\mathcal{M}$ increases the depth and the maximum negative value of potential also increase. Rarefactive

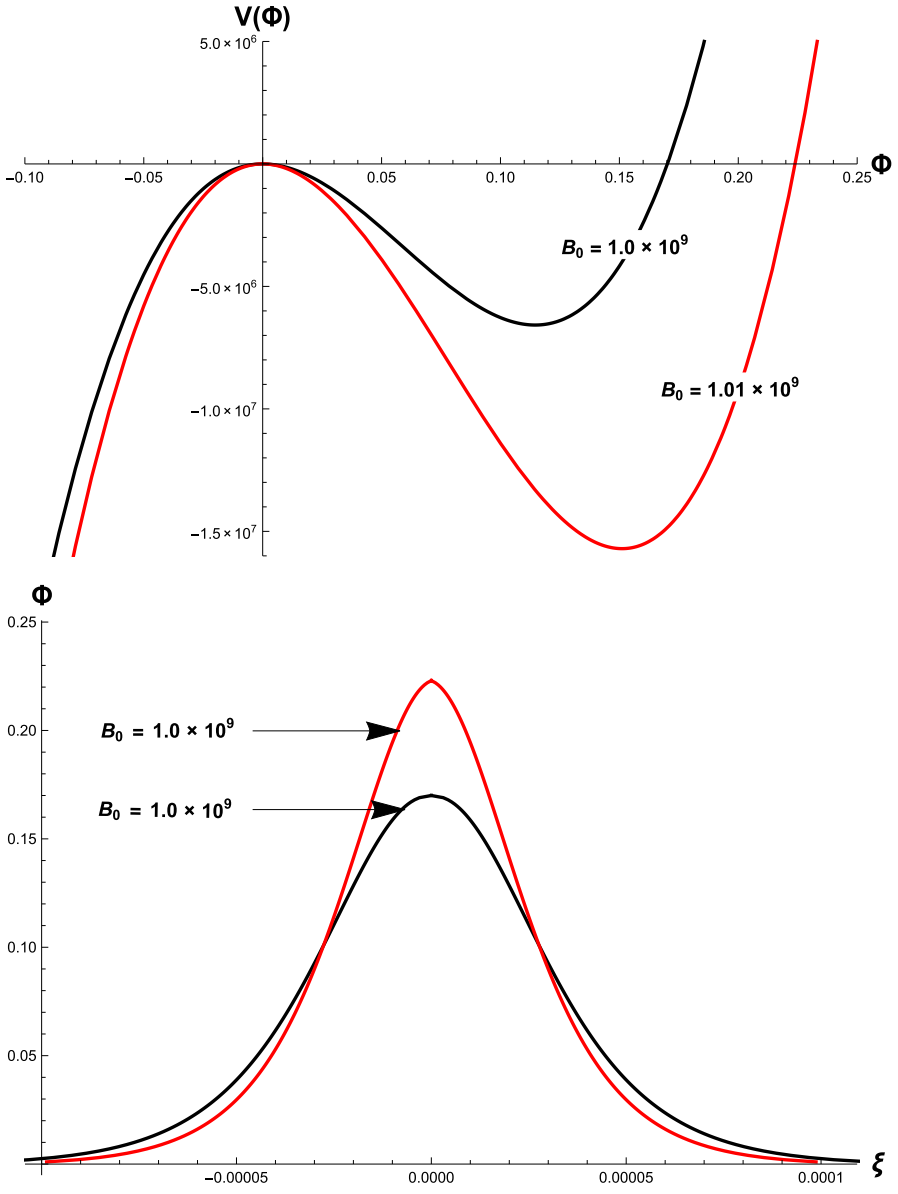

Fig. 21 Sagdeev potential (upper panel) and corresponding solitons (lower panel) with increasing magnetic field when $n = 2.5 \times 10^{26}$ cm^{-3} and $\kappa_n = -0.1$ cm^{-1}

solitons corresponding to the Sagdeev potentials in Fig. 14 are plotted in Fig. 15. We can see that amplitude of rarefactive solitons increases but width decreases as we increase the value of $\mathcal{M}$. Likewise, rarefactive Sagdeev potentials for different Mach numbers $\mathcal{M}$ when $\theta = \pi/9$ and $\theta = \pi/6$ are plotted in Figs. 16 and 17, respectively. These plots exhibit the same trend shown in Fig. 14, i.e. the depth and the maximum

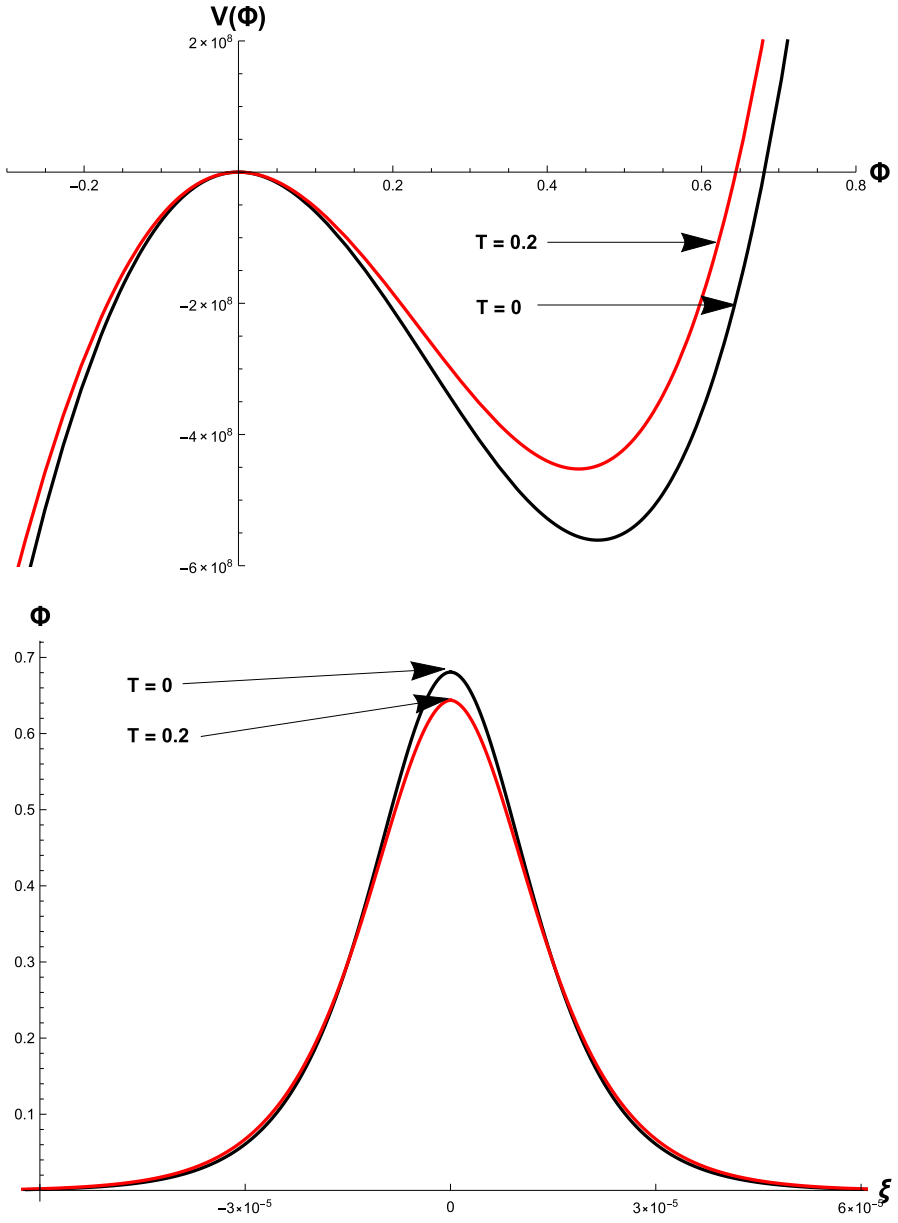

Fig. 22 Sagdeev potential (upper panel) for fully ($T = 0$) and partially degenerate ($T = 0.2$) quantum plasma and corresponding solitons (lower panel) when $B_0 = 1 \times 10^9$ G, $n = 2.15 \times 10^{26}$ cm^{-3} and $\kappa_n = -0.1$ cm^{-1}

negative value of Sagdeev potential increase as the Mach numbers $\mathcal{M}$ increases. In Fig. 18, we plot the rarefactive Sagdeev potential structures for two slightly different angles of propagation with identical Mach number. In Fig. 18, Sagdeev potential

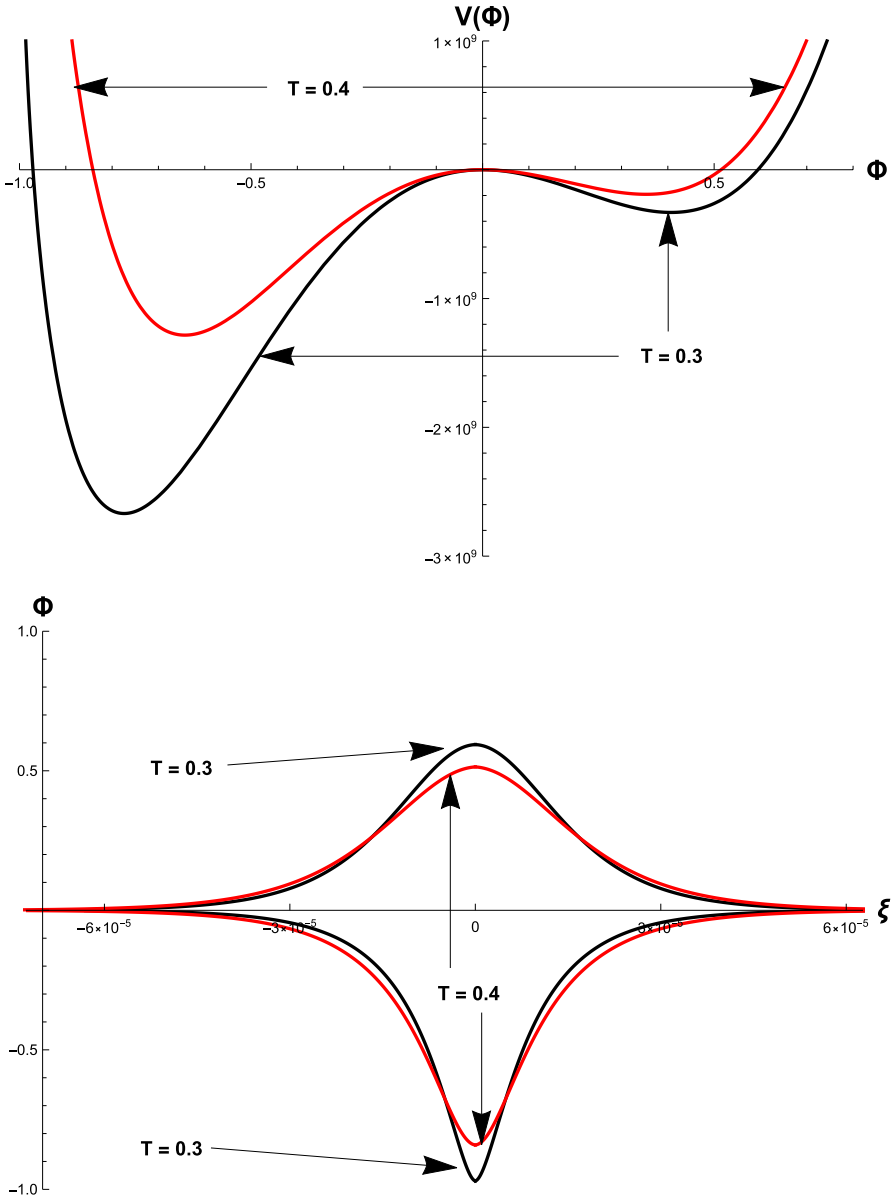

Fig. 23 Sagdeev potential (upper panel) with increasing temperature and corresponding solitons (lower panel) when $B_0 = 1 \times 10^9$ G, $n = 2.15 \times 10^{26}$ cm^{-3} and $\kappa_n = -0.1$ cm^{-1}

curves show that as the angle of propagation increases the depth and the maximum negative value of potential mitigate appreciably.

These results obtained in Figs. 12, 13, 14, 15, 16, 17 and 18 are summed up in Figs. 19 and 20 where minimum value of potential Φ_{min} is plotted against the Mach

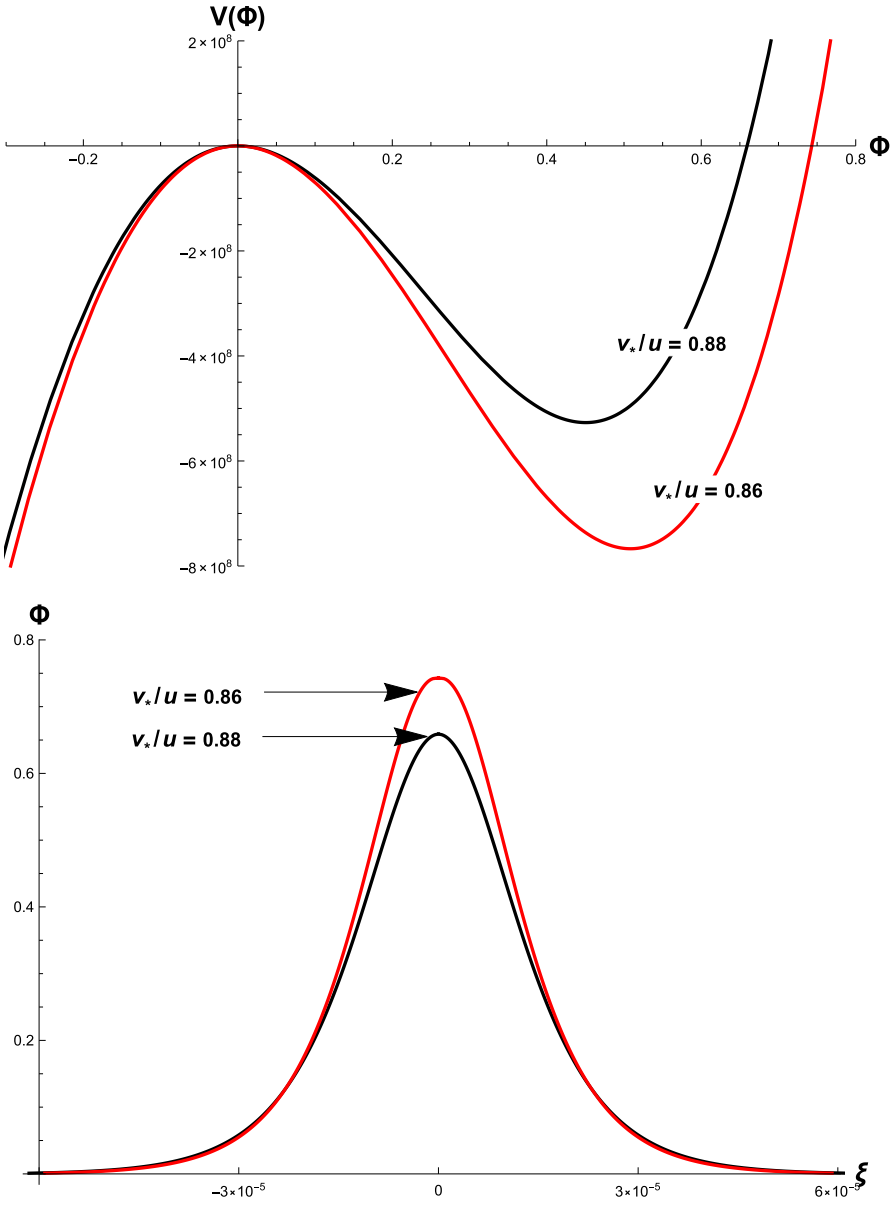

Fig. 24 Sagdeev potential (upper panel) with different ratios v_*/u and corresponding solitons (lower panel) when $B_0 = 1 \times 10^9$ G, $n = 2 \times 10^{26}$ cm^{-3} and $\kappa_n = -0.1$ cm^{-1}

number for different values of angle of propagation θ (Fig. 19) and drift velocity (Fig. 20). We can note that there is a certain range of Mach numbers corresponding to an angle of propagation and a drift velocity for which we can obtain the

rarefactive solitary structures. We can also note that the Φ_{min} decreases as Mach number increases for a certain angle of propagation as well as for a value of drift velocity.

We now plot Eq. (52) in the limiting case when $k_y \to 0$ in Figs. 21, 22, 23 and 24. In Fig. 21 (upper panel), Sagdeev potential plots show that the depth as well as the maximum value of potential increases as the magnetic field increases. This happens because the increasing magnetic field mitigates the nonlinearity coefficient and the coefficient of dispersion. Corresponding solitons are plotted in Fig. 21 (lower panel) in which soliton's amplitude increases but width decreases as the magnetic field increases. In Fig. 22 (upper panel), Sagdeev potential plots show that the depth as well as the maximum value of potential increases as the temperature decreases (within the range of quantum regime, i.e., $T < 1$). Corresponding solitons are plotted in Fig. 22 (lower panel) in which soliton's amplitude increases but width slightly decreases as the temperature decreases.

Figure 23 shows the Sagdeev potentials for partially degenerate quantum plasmas and corresponding solitons when we take larger temperature, i.e., $T > 0.2$ as compared to the temperatures taken in Figs. 21 and 22. Interestingly, we obtain both compressive and rarefactive Sagdeev potentials as shown in Fig. 23 (upper panel). We can see that as we increase the temperature, both Φ_{min} (for rarefactive Sagdeev potential) and Φ_{max} (for compressive Sagdeev potential) and corresponding depths decrease. Corresponding compressive and rarefactive solitons are plotted in Fig. 23 (lower panel) in which amplitude of both types of solitons decreases but the width increases with the increase in temperature. In Fig. 24 (upper panel), Sagdeev potentials are plotted for different values of drift velocity, $\boldsymbol{v}_*$, in which we can see that the depth as well as the maximum value of potential increases as the drift velocity $\boldsymbol{v}_*$ decreases. Corresponding solitons are plotted in Fig. 24 (lower panel) in which soliton's amplitude increases but width decreases slightly as the drift velocity $\boldsymbol{v}_*$ decreases.

6 Drift ion acoustic shock waves in spatially inhomogeneous magnetoplasmas with quantum trapping of electrons

In this section, we undertake to review our work on coupled drift ion acoustic shock waves with the inclusion of quantum trapping of electrons in magnetized plasmas (Fayyaz et al. 2020b). We once again consider a spatially nonuniform magnetized quantum plasma with fully degenerate electrons. The ions are once again considered to be cold and classical. Ion neutral collisions are also considered. The constant background magnetic field is considered in the z-direction, whereas the density inhomogeneity is taken in x direction. Thus, in this case the momentum equation is written as

$$m_i n_i \left(\partial_t + \boldsymbol{v_i}.\nabla\right)\boldsymbol{v_i} = e n_i \left(\boldsymbol{E} + \frac{1}{c}\boldsymbol{v_i} \times \boldsymbol{B_o}\right) - m_i n_i \nu_{in} \boldsymbol{v_i}. \tag{55}$$

Here ν_{in} is the ion neutral collisional frequency. As in the preceding section, using the drift approximation (Weiland 1999), we get for the velocity its parallel and perpendicular components for the low-frequency electrostatic wave, i.e., ($\Omega_{ci} \gg \partial_t$)

$$\left(\partial_t + \boldsymbol{v}_{\boldsymbol{E}}.\nabla_\perp + v_{iz}\partial_z\right)v_{iz} = -\frac{e}{m_i}\partial_z\varphi \tag{56}$$

$$\partial_t^2(1+\Phi)^{3/2} - \nu_{\rm in}\rho_i^2\partial_t\partial_y^2(1+\Phi) + \frac{3}{2}v_*\partial_y\partial_t(1+\Phi) - c_s^2\partial_z^2(1+\Phi) = 0. \tag{57}$$

where the third term of Eq. (57) is the collisional drift term. On the other hand, the adiabatically trapped degenerate electrons have number density given by Eq. (5). Following the same route as in the preceding section, we obtain the following nonlinear evolution equation:

$$\partial_t^2(1+\Phi)^{3/2} - \nu_{\rm in}\rho_i^2\partial_t\partial_y^2(1+\Phi) + \frac{3}{2}v_*\partial_y\partial_t(1+\Phi) - c_s^2\partial_z^2(1+\Phi) = 0. \tag{58}$$

Here the dispersion terms have been ignored. This is a new Burgers like nonlinear equation for a dissipative inhomogeneous plasma. As before, we introduce a new frame $\xi = \eta_y(y + \beta z - vt)$, where $\beta = \eta_z/\eta_y = \eta\sin\theta/\eta\cos\theta$, θ is the angle of propagation and η_y,η_z are the nonlinear wavenumbers along y and z-axis, respectively, $v = \Omega/\eta_y$ is the velocity and Ω is the frequency of the nonlinear structure. Setting $\Psi = 1 + \Phi$, we obtain the following dimensionless form of Eq. (59):

$$v^2\frac{{\rm d}^2\Psi^{3/2}}{{\rm d}\xi^2} + \frac{\nu_{\rm in}\rho_i^2\eta}{c_{\rm s}}v\frac{{\rm d}^3\Psi}{{\rm d}\xi^3} - \left(\beta^2 + \frac{3}{2}vv_*\right)\frac{{\rm d}^2\Psi}{{\rm d}\xi^2} = 0. \tag{59}$$

Normalizing $v = v/c_s$ and using the boundary conditions $\xi \to \infty$, $\Psi \to \Psi_{\rm R}$; $\xi \to -\infty$, $\Psi \to \Psi_{\rm L}$ and ${\rm d}_\xi^n\Psi \to 0$ where $\Psi_{\rm R}$ and $\Psi_{\rm L}$ are the right-hand and left-hand boundary conditions, respectively (Cameron 2011). We can integrate Eq. (59) twice. The integration constant the condition

$$v^2\Psi_{\rm R}^{3/2} - \left(\beta^2 + \frac{3}{2}vv_*\right)\Psi_{\rm R} = c_2 = v^2\Psi_{\rm L}^{3/2} - \left(\beta^2 + \frac{3}{2}vv_*\right)\Psi_{\rm L}. \tag{60}$$

The value of normalized Φ ranges from ±1; therefore, we get $\Psi_{\rm R} = 2$ and $\Psi_{\rm L} = 0$. Solving Eq. (60) for c_2 and v, we get

$$v = \frac{1}{8}\left[3\sqrt{2}v_* \pm \sqrt{18v_*^2 + 32\sqrt{2}\beta^2}\right] \tag{61}$$

$$c_2 = \frac{\left[3\sqrt{2}v_* + \sqrt{18v_*^2 + 32\sqrt{2}\beta^2}\right]^2}{16\sqrt{2}} - 2\left[\beta^2 + \frac{3}{16}v_*\left(3\sqrt{2}v_* + \sqrt{18v_*^2 + 32\sqrt{2}\beta^2}\right)\right] \tag{62}$$

Using Eqs. (61) and (62) in Eq. (60), we obtain

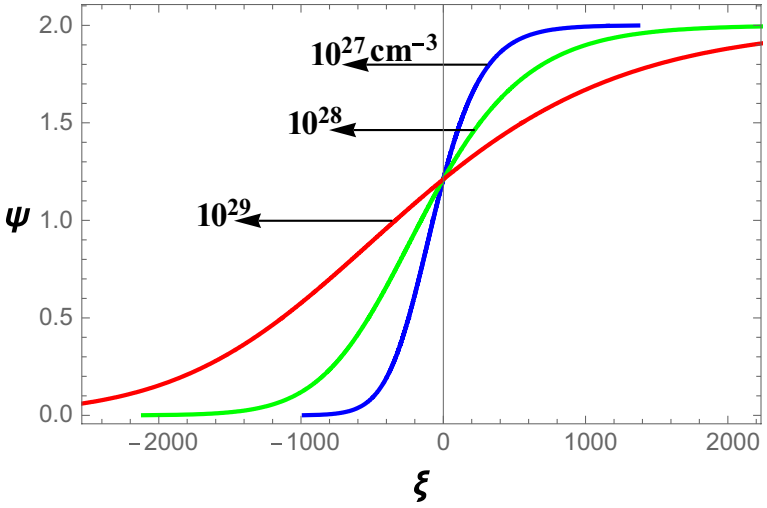

Fig. 25 Shock profiles for different number densities when $B_o = 10^{10}$ G, $\nu_{in} = 1 \times 10^{15}$ s^{-1}, $v_*/c_s = 0.4$ and $\theta = 10^0$

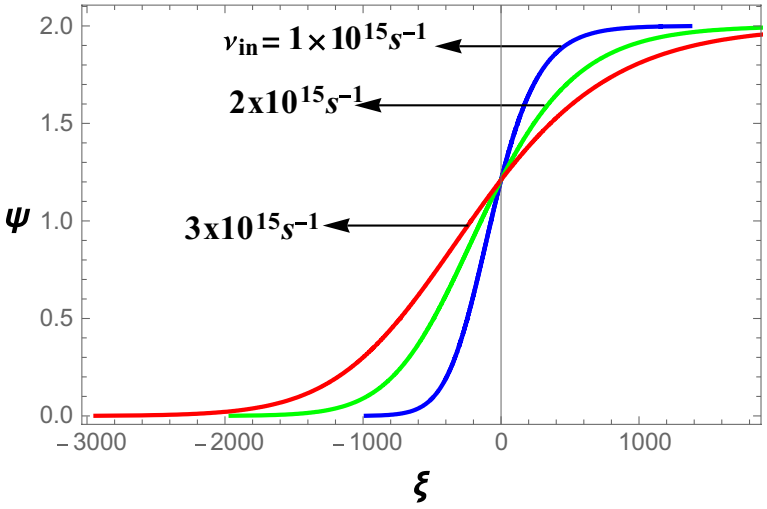

Fig. 26 Shock profiles for different collisional frequencies when $n_o = 10^{27}$cm^{-3}, $B_o = 10^{10}$ G, $v_*/c_s = 0.4$ and $\theta = 10^0$

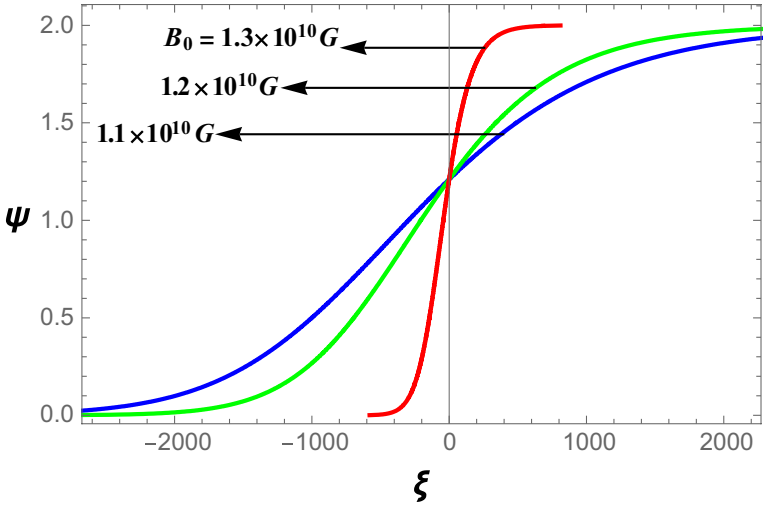

Fig. 27 Shock profiles for different magnetic fields when $n_o = 10^{27}\text{cm}^{-3}$, $\nu_{in} = 1\times10^{15}\ \text{s}^{-1}$, $v_*/c_s = 0.4$ and $\theta = 10^0$

$$d\xi = \frac{\nu_{in}c_s\eta}{\Omega_{ci}^2}\left(\frac{v}{\left(\beta^2+\frac{3}{2}v\nu_*\right)\Psi - v^2\Psi^{3/2}+c_2}\right)d\Psi. \tag{63}$$

Integrating Eq. (14) yields a solution given as follows:

$$\xi = -\frac{2\sqrt{2}\nu_{in}c_s\eta\left(3\nu_* + \sqrt{9\nu_*^2+16\sqrt{2}\beta^2}\right)}{\Omega_{ci}^2\left(9\sqrt{2}\nu_*^2+16\beta^2+3\nu_*\sqrt{18\nu_*^2+32\sqrt{2}\beta^2}\right)} \times\left(2\text{Log}\left[9\nu_*^2\left(\sqrt{2}-\sqrt{\Psi}\right)+3\nu_*\sqrt{9\nu_*^2+16\sqrt{2}\beta^2}\left(\sqrt{2}-\sqrt{\Psi}\right)-8\beta^2\left(-2+\sqrt{2\Psi}\right)\right]-\text{Log}\Psi\right) \tag{64}$$

We have numerically investigated Eq. (64) and found that it admits shock solution.

6.1 Results and discussion

In the present section, we numerically investigated the positive root of Eq. (64) which yields the shock structure by considering the numerical values of magnetic field and number density for dense astrophysical plasmas given in Sect. 5.2. In Fig. 25, we plot the shock structures for different values of number density. We can see that the electrostatic shock amplitude remains the same, but steepness decreases with the increase in number density. In Fig. 26, we plot the shock structures for different values of collision frequency ν_{in}. We can see that the electrostatic shock

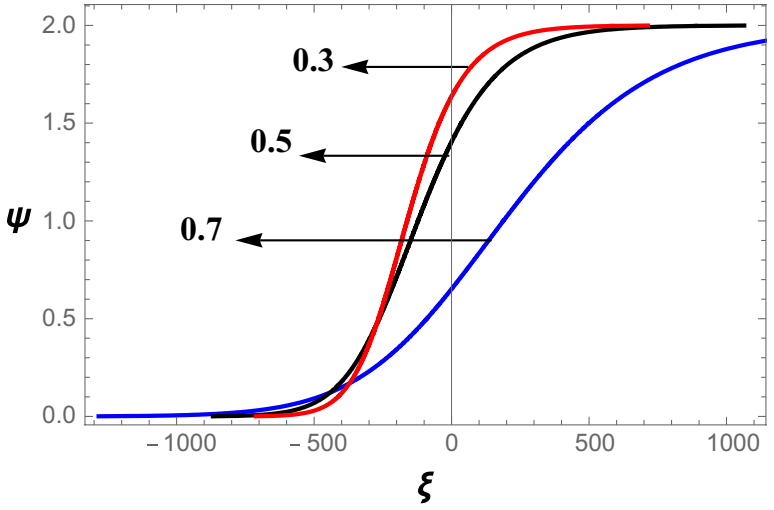

Fig. 28 Shock profiles for different values of inhomogeneities when $n_o = 10^{27}\,\mathrm{cm}^{-3}$, $B_o = 10^{10}\,\mathrm{G}$, $\nu_{in} = 1 \times 10^{15}\mathrm{s}^{-1}$ and $\theta = 10^0$

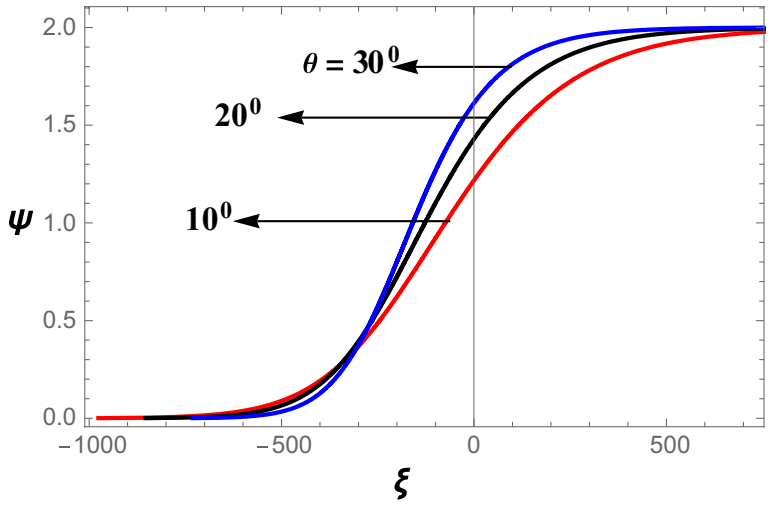

Fig. 29 Shock profiles for angle of propagations when $n_o = 10^{27}\mathrm{cm}^{-3}$, $\nu_{in} = 1 \times 10^{15}\mathrm{s}^{-1}$, $v_*/c_s = 0.4$ and $B_o = 10^{10}\,\mathrm{G}$

amplitude remains the same, but steepness decreases with the increase in collision frequency ν_{in}. We also probe the impact of magnetic field on the electrostatic shock structures in Fig. 27. It can be noted that the electrostatic shock amplitude as well as the steepness increases with the increase in magnetic field.

We have applied our results to neutron stars where the quantum effects are expected to dominate. The plot of Eq. (65) for the positive root of v has

yielded compressive shock structures which we have investigated numerically by using the standard parameters of dense astrophysical plasmas (neutron stars) whose dynamics are governed by quantum effects i.e., $n_o \sim 10^{26} - 10^{29}\text{cm}^{-3}$ and $B_o \sim 10^9 - 10^{11}\text{G}$. We probe the impact of the varying number density n_o, collisional frequency ν_{in} and magnetic field strength B_o on the shock structure. From Figs. 25 and 26, we see that the fall of the electrostatic potential becomes sharp as the number density and collisional frequency decrease respectively which are evident from Eq. (15). On the contrary, from Fig. 27 we see that the steepness of the shock wave enhances with the increase in magnetic field strength.

The variation in drift velocity v_* (spatial inhomogeneity) is also observed to modify the shock profile as shown in Fig. 28. The steepness of the shock is observed to enhance with the increase in drift velocity but there is no observed change in the shock amplitude. However, if the angle of propagation is varied, the shock front becomes sharper, but the height of the shock remains the same as the angle of propagation increases (Fig. 29).

Before we go on and conclude the review, we would like to comment on the question as to how quantum effects be observed in these extreme environments. We get to know about the interior of white dwarf stars from the electromagnetic radiation that comes from them. It provides us information about their physical properties and dynamics (Dwarfs and Stars 1983). So far, more than two hundred pulsating white dwarf stars have been observed. The theoretical construct of these pulsations is widely accepted and the discipline of white-dwarf asteroseismology helps us determine the rotation period, mass, and equation of state of these stars (Winget and Kepler 2008; Fontaine and Brassard 2008). Besides gravity waves, the theory surmises the existence of acoustic modes (p-modes). Ostriker (1971) conjectured them long time ago but they yet to be observed (Silvotti et al. 2011). It does not imply non-existence of p-mode oscillations and lack of observation may be associated with the motion below the detection limit (Eliasson and Shukla 2011). The possible formation of nonlinear structures in the case of extreme events such as supernova explosions or the collision of white dwarfs with other astrophysical bodies has also been proposed (Eliasson and Shukla 2011).

Employing the intense laser pulses, investigations have been made about the radiative blast waves in atomic cluster media (Norreys et al. 2009). It has been shown that atomic clusters are very efficient absorbers of intense laser radiation and can be gainfully used to create high energy density plasmas that drive strong shocks (> Mach 50) and radiative blast waves. This has engendered the possibility of scaling the experiments to astrophysical phenomena that have 15–20 greater orders of magnitude length and time scales. The radiative blast waves thus hold a lot of promise to understand supernova remnants and the physics governing their dynamics under controlled conditions in the laboratory (Norreys et al. 2009). Note that the in-situ observations of waves in dense plasmas in extreme environments are very difficult. However, the rapid development of laser technology as mentioned above would hopefully make it possible for us to compare the theory with experiments.

7 Conclusions

In this review, we have presented a comprehensive view of the effects of trapping on the formation of solitary and shock waves in both homogeneous and inhomogeneous quantum plasmas.

First, we have presented the simplest case of quantum trapping and explained how it differs from its classical counterpart and enunciated in detail how trapping was done by Gurevich (1968) for the adiabatic electron capture in classical plasmas by dividing the integrals into free and trapped particles.

Next, we have considered the case of trapping in relativistically degenerate quantum plasmas. The expression of Sagdeev potential has been studied numerically and graphs have been plotted to illustrate the dependence of propagation characteristics of solitary waves on the physical parameters. The importance of the work in ultra-strong laser plasma interactions has been pointed out and it is expected to help in comprehending dense astrophysical objects like white dwarf stars. In the limiting case, the expression for the non-relativistic electron trapping has been retrieved.

Further, we have studied the linear and nonlinear structure formation in fully and partially degenerate plasmas with the inclusion of quantizing magnetic field. We first study the linear dispersion characteristics (LDCs) of the modified ion acoustic wave (IAW). Contrary to the classical case, the parallel propagating wave (i.e., wave propagating along the ambient magnetic field) has been found to depend on the magnetic field. We have numerically explored the effect of Mach number, magnetic field, and electron temperature on the LDCs of the quantum IAW in the presence of quantizing field. The effect of the above-mentioned plasma parameters on the propagation of nonlinear solitary structures has also been investigated. It has been reported that the system under consideration allows only the formation of hump solitary structures for fully degenerate plasmas while for the case of partially degenerate plasmas, the formation of both hump and dip solitary structures has been reported. The relevance of the investigation with special reference to ultra-strong laser plasma interactions and white dwarfs has also been highlighted.

Next, we have studied nonlinear coupled drift ion acoustic dispersive structures in fully degenerate, spatially nonuniform magnetoplasmas. Using QMHD model, we have come up with a new nonlinear equation representing the coupling of pure drift vortex mode with the parallel propagating acoustic mode in the presence of fractional nonlinearity that arises owing to electron trapping in degenerate plasmas. By dint of Sagdeev potential approach, we have investigated the coupled drift acoustic solitary structures. We have presented the numerical investigation by using the neutron star parameters and it has been found that rarefactive solitary structures could exist for the chosen parameters. These solitary structures have been shown to depend on the angle of propagation and inhomogeneity. The study can be usefully employed in variegated environments in astrophysical plasmas. It extends our understanding of dealing with nonlinearities which appears as $(1+\Phi)^{3/2}$ as opposed to $\Phi^{3/2}$ term which we encounter in classical trapping. We have also retrieved the pure drift mode case in the limit when k_z goes to zero.

Finally, one-dimensional Burgers like nonlinear evolution equation for the ion drift wave has been obtained for an inhomogeneous, collisional quantum magnetoplasma in the presence of weak gradient in background density and Gurevich (Gurevich 1968) like trapping. An analytical solution to this equation has been obtained (which turns out to be a shock solution) and the dependence of the shock strength on the background number density, collisional frequency, ambient magnetic field, background density inhomogeneity, and angle of propagation has been investigated. Like for the solitary case, fractional nonlinearity for the quantum trapping has been dealt with here and all the new features have been highlighted in detail.

References

H. Abbasi, N. Tsintsadze, D. Tskhakaya, Influence of particle trapping on the propagation of ion cyclotron waves. Phys. Plasmas **6**(6), 2373–2379 (1999)

S. Ali, P. Shukla, Streaming instability in quantum dusty plasmas. Eur. Phys. J. D **41**(2), 319–324 (2007)

S. Ali et al., Linear and nonlinear ion-acoustic waves in an unmagnetized electron-positron-ion quantum plasma. Phys. Plasmas **14**(8), 082307 (2007)

L. Ang, T. Kwan, Y. Lau, New scaling of Child-Langmuir law in the quantum regime. Phys. Rev. Lett. **91**(20), 208303 (2003)

M. Ayub, H. Shah, M. Qureshi, Trapping effects in a self-gravitating quantum dusty plasma. Phys. Scr. **84**(4), 045505 (2011)

S. Balberg, S.L., Shapiro, The properties of matter in white dwarfs and neutron stars. arXiv preprint astro-ph/0004317 (2000a)

Balberg, S., Shapiro, S.L., The properties of condensed matter in white dwarfs and neutron stars. In: Handbook of elastic properties of solids, liquids, and gases. **4**. (2000b)

I.B. Bernstein, J.M. Greene, M.D. Kruskal, Exact nonlinear plasma oscillations. Phys. Rev. **108**(3), 546 (1957)

D. Bohm, A suggested interpretation of the quantum theory in terms of" hidden" variables. I. Phys. Rev. **85**(2), 166 (1952)

D. Bohm, D. Pines, A collective description of electron interactions: III. Coulomb interactions in a degenerate electron gas. Phys. Rev. **92**(3), 609 (1953)

M. Cameron, *Notes on the Burgers Equation* (University of Maryland, 2011)

G. Chabrier, F. Douchin, A. Potekhin, Dense astrophysical plasmas. J. Phys. Condens. Matter **14**(40), 9133 (2002)

S. Chandrasekhar, XLVIII. The density of white dwarf stars. Lond. Edinb. Dublin Philos. Mag. J. Sci. **11**(70), 592–596 (1931)

P. Chatterjee et al., Effect of ion temperature on arbitrary amplitude ion acoustic solitary waves in quantum electron-ion plasmas. Phys. Plasmas **16**(4), 042311 (2009)

A.-L. Chian, Effect of ion dynamics on relativistic nonlinear plasma oscillations. Plasma Phys. **24**(1), 19 (1982)

J. Daniel, T. Tajima, Outbursts from a black hole via alfvén wave to electromagnetic wave mode conversion. Astrophys. J. **498**(1), 296 (1998)

V. Demchenko, I. El-Naggar, On hybrid resonances in non-homogeneous magneto-active plasma. Physica **58**(1), 144–160 (1972)

L. Demeio, Quantum corrections to classical BGK modes in phase space. Transport Theory Stat. Phys. **36**(1–3), 137–158 (2007)

W. Dwarfs, N. Stars, *The Physics of Compact Objects* (Wiley, 1983)

B. Eliasson, P. Shukla, The formation of electrostatic shocks in quantum plasmas with relativistically degenerate electrons. EPL (Europhysics Letters) **97**(1), 15001 (2011)

A. Fayyaz et al., Nonlinear drift ion acoustic waves in degenerate plasmas with adiabatic trapping. Phys. Scr. **95**(4), 045609 (2020a)

A. Fayyaz et al., Coupled drift ion acoustic shock waves with trapped electrons in quantum magnetoplasma. Phys. Scri. **95**(8), 085602 (2020b)

G. Fontaine, P. Brassard, The pulsating white dwarf stars. Publ. Astron. Soc. Pac. **120**(872), 1043 (2008)
S. Ghosh, G. Lakhina, Anomalous width variation of rarefactive ion acoustic solitary waves in the context of auroral plasmas. Nonlinear Process. Geophys. **11**(2), 219–228 (2004)
P. Goldreich, W.H. Julian, Pulsar electrodynamics. Astrophys. J. **157**, 869 (1969)
A. Gurevich, Distribution of captured particles in a potential well in the absence of collisions. Sov. Phys. JETP **26**(3), 575–580 (1968)
F. Haas, *Quantum Plasmas: An Hydrodynamic Approach*, vol. 65 (Springer Science & Business Media, 2011)
F. Haas, S. Mahmood, Nonlinear ion-acoustic solitons in a magnetized quantum plasma with arbitrary degeneracy of electrons. Phys. Rev. E **94**(3), 033212 (2016)
F. Haas, G. Manfredi, M. Feix, Multistream model for quantum plasmas. Phys. Rev. E **62**(2), 2763 (2000)
Q. Haque, H. Saleem, Ion acoustic vortices in quantum magnetoplasmas. Phys. Plasmas **15**(6), 064504 (2008)
H. Haug, S.W. Koch, *Quantum Theory of the Optical and Electronic Properties of Semiconductors* (World Scientific Publishing Company, 2009)
M. Iqbal et al., Nonlinear density excitations in electron-positron-ion plasmas with trapping in a quantizing magnetic field. Phys. Plasmas **24**(1), 014503 (2017)
I.U.R.L.V. Klimontovich, *Concerning the Spectra of Systems of Interacting Particles* (US Atomic Energy Commission, 1952)
D. Koester, G. Chanmugam, Physics of white dwarf stars. Rep. Progress Phys. **53**(7), 837 (1990)
H. Kuehl, C. Zhang, Effect of ion drift on arbitrary-amplitude ion-acoustic solitary waves. Phys. Fluids B Plasma Phys. **3**(3), 555–559 (1991)
L. Landau, E. Lifshitz, *Statistical physics Pergamon* (Elsevier, 1980)
N.C. Lee, C.R. Choi, Ion-acoustic solitary waves in a relativistic plasma. Phys. Plasmas **14**(2), 022307 (2007)
M. Leontovich, *Reviews of Plasma Physics* (Springer Science & Business Media, 2012)
A. Luque, H. Schamel, Electrostatic trapping as a key to the dynamics of plasmas, fluids and other collective systems. Phys. Rep. **415**(5–6), 261–359 (2005)
A. Luque, H. Schamel, R. Fedele, Quantum corrected electron holes. Phys. Lett. A **324**(2–3), 185–192 (2004)
J.H. Luscombe, A.M. Bouchard, M. Luban, Electron confinement in quantum nanostructures: self-consistent Poisson-Schrödinger theory. Phys. Rev. B **46**(16), 10262 (1992)
S. Mahmood, W. Masood, Electron acoustic solitary waves in unmagnetized two electron population dense plasmas. Phys. Plasmas **15**(12), 122302 (2008)
S. Mahmood, A. Mushtaq, Quantum ion acoustic solitary waves in electron–ion plasmas: a Sagdeev potential approach. Phys. Lett. A **372**(19), 3467–3470 (2008)
A. Mamun, Effects of ion temperature on electrostatic solitary structures in nonthermal plasmas. Phys. Rev. E **55**(2), 1852 (1997)
G. Manfredi, How to model quantum plasmas. Fields Inst. Commun. **46**, 263–287 (2005)
G. Manfredi, M. Feix, Theory and simulation of classical and quantum echoes. Phys. Rev. E **53**(6), 6460 (1996)
G. Manfredi, P.-A. Hervieux, Autoresonant control of the many-electron dynamics in nonparabolic quantum wells. Appl. Phys. Lett. **91**(6), 061108 (2007)
P.A. Markowich, C.A. Ringhofer, C. Schmeiser, *Semiconductor Equations* (Springer Science & Business Media, 2012)
W. Masood, Obliquely propagating low frequency electromagnetic shock waves in two dimensional quantum magnetoplasmas. Phys. Plasmas **16**(4), 042314 (2009a)
W. Masood, Drift ion acoustic solitons in an inhomogeneous 2-D quantum magnetoplasma. Phys. Lett. A **373**(16), 1455–1459 (2009b)
W. Masood et al., Coupled nonlinear drift and ion acoustic waves in dense dissipative electron-positron-ion magnetoplasmas. Phys. Plasmas **16**(11), 112302 (2009)
W. Masood, N. Jehan, A.M. Mirza, A new equation in two dimensional fast magnetoacoustic shock waves in electron-positron-ion plasmas. Phys. Plasmas **17**(3), 032314 (2010)
W. Masood et al., A nonlinear model for magnetoacoustic waves in dense dissipative plasmas with degenerate electrons. Phys. Plasmas **21**(10), 102311 (2014)
F.C. Michel, Theory of pulsar magnetospheres. Rev. Mod. Phys. **54**(1), 1 (1982)
S. Mola, G. Manfredi, M. Feix, Expansion of a quantum electron gas. J. Plasma Phys. **50**(1), 145–162 (1993)

A. Mushtaq, A. Qamar, Parametric studies of nonlinear magnetosonic waves in two-dimensional quantum magnetoplasmas. Phys. Plasmas **16**(2), 022301 (2009)
A. Mushtaq, H. Shah, Study of non-Maxwellian trapped electrons by using generalized (r, q) distribution function and their effects on the dynamics of ion acoustic solitary wave. Phys. Plasmas **13**(1), 012303 (2006)
Y. Nejoh, Double layers, spiky solitary waves, and explosive modes of relativistic ion-acoustic waves propagating in a plasma. Phys. Fluids B Plasma Phys. **4**(9), 2830–2840 (1992)
P. Norreys et al., Intense laser-plasma interactions: new frontiers in high energy density physics. Phys. Plasmas **16**(4), 041002 (2009)
J.A. Orosz et al., An optical precursor to the recent X-ray outburst of the black hole binary GRO J1655–40. Astrophys. J. Lett. **478**(2), L83 (1997)
J.P. Ostriker, Recent developments in the theory of degenerate dwarfs. Annu. Rev. Astron. Astrophys. **9**(1), 353–366 (1971)
D. Pines, Quantum plasma physics. J. Nucl. Energy Part C Plasma Phys. **2**(5), 5 (1961)
L. Pitaevskii, E. Lifshitz, *Physical kinetics*, vol. 10 (Butterworth-Heinemann, 2012)
A. Pointon, *Introduction to Statistical Physics* (Longman, London and New York, 1980)
H. Ren et al., Electrostatic drift modes in quantum dusty plasmas with Jeans terms. Phys. Plasmas **16**(10), 103705 (2009)
R. Sagdeev, M. Leontovich, *Reviews of Plasma Physics* (Consultants Bureau New York, 1966)
O. Sah, J. Manta, Nonlinear electron-acoustic waves in quantum plasma. Phys. Plasmas **16**(3), 032304 (2009)
A. Saha, B. Pradhan, S. Banerjee, Bifurcation analysis of quantum ion-acoustic kink, anti-kink and periodic waves of the Burgers equation in a dense quantum plasma. Eur. Phys. J. plus **135**(2), 1–13 (2020)
B. Sahu, R. Roychoudhury, Electron-acoustic solitary waves and double layers in a relativistic electron-beam plasma system. Phys. Plasmas **11**(5), 1947–1954 (2004)
B. Sahu, R. Roychoudhury, Electron acoustic solitons in a relativistic plasma with nonthermal electrons. Phys. Plasmas **13**(7), 072302 (2006)
H. Shah, M. Qureshi, N. Tsintsadze, Effect of trapping in degenerate quantum plasmas. Phys. Plasmas **17**(3), 032312 (2010)
H. Shah et al., Effects of trapping and finite temperature in a relativistic degenerate plasma. Phys. Plasmas **18**(10), 102306 (2011)
H. Shah et al., Effect of trapping in a degenerate plasma in the presence of a quantizing magnetic field. Phys. Plasmas **19**(9), 092304 (2012)
H. Shah, W. Masood, Z. Ali, Adiabatic trapping in coupled kinetic Alfvén-acoustic waves. Phys. Plasmas **20**(3), 032301 (2013)
H. Shah et al., Drift solitary structures in inhomogeneous degenerate quantum plasmas with trapped electrons. Astrophys. Sp. Sci. **350**(2), 615–622 (2014)
B. Shokri, S. Khorashady, Pramana (2003). https://doi.org/10.1007/BF02704506
B. Shokri, A. Rukhadze, Quantum surface wave on a thin plasma layer. Phys. Plasmas **6**(9), 3450–3454 (1999a)
B. Shokri, A. Rukhadze, Quantum drift waves. Phys. Plasmas **6**(12), 4467–4471 (1999b)
P.K. Shukla, B. Eliasson, Recent developments in quantum plasma physics. Plasma Phys. Control. Fusion **52**(12), 124040 (2010a)
P.K. Shukla, B. Eliasson, Nonlinear aspects of quantum plasma physics. Phys. Usp. **53**(1), 51 (2010b)
P. Shukla, B. Eliasson, Colloquium: Nonlinear collective interactions in quantum plasmas with degenerate electron fluids. Rev. Mod. Phys. **83**(3), 885 (2011)
P.K. Shukla, L. Stenflo, New drift modes in a nonuniform quantum magnetoplasma. Phys. Let. A **357**(3), 229–231 (2006)
N. Shukla et al., Ion streaming instability in a quantum dusty magnetoplasma. Phys. Plasmas **15**(4), 044503 (2008)
P. Shukla, A. Mamun, D. Mendis, Nonlinear ion modes in a dense plasma with strongly coupled ions and degenerate electron fluids. Phys. Rev. E **84**(2), 026405 (2011)
H. Siddiqui, H. Shah, N. Tsintsadze, Effect of trapping on vortices in plasma. J. Fusion Energy **27**(3), 216–224 (2008)
R. Silvotti et al., Search for p-mode oscillations in DA white dwarfs with VLT-ULTRACAM-I. Upper limits to the p-modes. Astron. Astrophys. **525**, A64 (2011)

V.O. Strasser, Relativistic arbitrary-amplitude electrostatic solitons in a plasma. Phys. Rev. E **53**(5), 5194 (1996)
N.-D. Suh, M.R. Feix, P. Bertrand, Numerical simulation of the quantum Liouville-Poisson system. J. Comput. Phys. **94**(2), 403–418 (1991)
Tsintsadze, L.N. *Quantization and excitation of longitudinal electrostatic waves in magnetized quantum plasmas*. In: *AIP Conference Proceedings*, vol 1306 (American Institute of Physics, 2010), pp. 89
N. Tsintsadze, E. Tsikarishvili, Parametric instabilities in relativistic plasma. Astrophys. Sp. Sci. **39**(1), 191–199 (1976)
N. Tsintsadze, D. Tskhakaya, On the theory of electrosound waves in a plasma. Sov. Phys. JETP **72**, 480 (1977)
N. Tsintsadze et al., Nonlinear screening effect in an ultrarelativistic degenerate electron-positron gas. Phys. Plasmas **16**(11), 112307 (2009)
Tyshetskiy, Y.O., Vladimirov, S., Kompaneets, R. *Unusual physics of quantum plasmas.* Вопросы атомной науки и техники, (2013)
H. Van Horn, Dense astrophysical plasmas. Science **252**(5004), 384–389 (1991)
M.A. Wahab, *Solid State Physics: Structure and Properties of Materials* (Alpha Science Int'l Ltd., 2005)
J. Weiland, *Collective Modes in Inhomogeneous Plasmas: Kinetic and Advanced Fluid Theory* (CRC Press, 1999)
D. Winget, S. Kepler, Pulsating white dwarf stars and precision asteroseismology. Annu. Rev. Astron. Astrophys. **46**, 157–199 (2008)
E. Witt, W. Lotko, Ion-acoustic solitary waves in a magnetized plasma with arbitrary electron equation of state. Phys. Fluids **26**(8), 2176–2185 (1983)
M. Yahia, I. Azzouz, W. Moslem, Quantum effects in electron beam pumped GaAs. Appl. Phys. Lett. **103**(8), 082105 (2013)
M. Yalabik et al., Quantum mechanical simulation of charge transport in very small semiconductor structures. IEEE Trans. Electron Devices **36**(6), 1009–1013 (1989)
M. Zobaer et al., K-dV and Burgers' equations on DA waves with strongly coupled dusty plasma. Astrophys. Sp. Sci. **346**(2), 351–357 (2013)